PHYSICS EDUCATION

INDIAN ASSOCIATION OF PHYSICS TEACHERS

IAPT

Absolute voltage balance diagram

Volume 31, Number 1

In this Issue

EDITORIAL

It is a pleasure to publish the issue 31.1 of Physics Education. This issue covers many interesting problems like an object moving on a rotating spherical surface, Doppler shift of de Broglie waves, measurement of Planck constant, explaining pressure in the context of chemical thermodynamics, LED irradiance, near filed communication and so on. Determination of magnetic dipole moment of permanent disc magnets is the subject of physics through lab. I am sure this issue will be of interest to teachers and students alike.

Finally I wish you a very happy reading!

Pramod S. Joag.

Chief Editor, Physics Education
Chief-editor@physedu.in,
pramod@physics.unipune.ac.in

Velocity Change Calculation for an Object Moving on a Rotating Spherical Surface

Jean C. Piquette

72 Botelho Drive, Portsmouth, Rhode Island 02871 USA

jpiquette@verizon.net

Abstract

If an object is constrained to move on the surface of a sphere that is rotating at constant angular velocity, it is well known that within the rotating frame Coriolis and centrifugal accelerations appear. Assuming that there are no physical forces acting on the object that are directed tangentially, one might suppose that the change in velocity of the object over a finite time interval could thus be determined by integrating the sum of the Coriolis and centrifugal accelerations over that time interval. This procedure, however, does not yield the correct value for the velocity change. Owing to performing the calculation in spherical coordinates, additional acceleration contributions must also be included. The constraint forces cannot be the sources of these additional contributions, because the constraints are directed radially, while the additional accelerations are directed tangentially. The required additional acceleration terms are derived from first principles in a manner that would be suitable for presentation in either an undergraduate or graduate mechanics course.

1. Introduction

The problem of interest is the calculation of the components of the velocity change that occur over a finite time interval for an object moving on the surface of a rotating sphere, as determined within a reference frame that is rotating with the sphere. The object is constrained to remain on the sphere's surface, and it is assumed no physical forces act on the object in the tangential direction. For definiteness, the sphere is assumed in example calculations to be similar to the Earth. However, the sphere is assumed to always remain exactly spherical, and there is no atmosphere. The sphere is assumed to complete one full rotation is exactly 24 hours, and to have a radius of exactly 4000

miles. The only physical forces that are present are radially directed, and include gravity and the normal force of the spherical surface on the object. It is well known that under the conditions of interest, fictitious accelerations arise within the rotating frame. These are the Coriolis and centrifugal accelerations. One might suppose that since these two fictitious accelerations are the only

There has been much work done in the area of noninertial frames [1-10]. Reference 1 considers the problem of an object moving on the Earth's surface in the absence of tangential physical forces. However, the problem was solved numerically, not analytically. Here the exact analytical solution is presented, although for a less general case. The problem is also considered analytically in Ref. 2, including radial motion. The calculation of velocity changes was also considered in Ref. 2, although the results given there are expressed in approximate expansions, not the exact analytical results given here. It is worthwhile noting that the need to include accelerations other than Coriolis and centrifugal were also found to be required in Ref. 2. This result is termed a "curvilinear effect."

The behavior of an object in a rotating two-dimensional frame is considered in Ref. 3. It can be worthwhile for students to consider the methods of this reference before moving on to the more difficult problem of motion on a curved surface. The problem of motion in a spherical noninertial frame is considered in Ref. 4 through Ref. 9. These references consider the more difficult case in which the motion in the radial direction is unconstrained. They also consider the presence of additional forces such as air resistance. The work presented in Ref. 10 is

ones that arise, it should be possible to compute the desired velocity change components simply by integrating the components of these two fictitious accelerations over the time interval of interest. This procedure, however, does not produce the correct result. This fact can be valuable to discuss with students when presenting the Coriolis concept, and to include in more general discussions of noninertial frames.

worthwhile because it describes demonstrations and experiments that can be done in the classroom and also used in a physics laboratory course.

In section 2 the approach used in determining the velocity change calculation of interest is described, and the two coordinate systems used here are presented. The equations of motion in the rotating frame are given in section 3. The expressions for the velocity change components over a finite time interval are developed in section 4, and thus the principal results of this work are contained in this section. The results of section 4 are discussed in section 5 in terms of a simple example that illustrates why integrating over only the Coriolis and centrifugal accelerations produces the wrong result. A more complicated special-case example is described and the exact analytical solution of it are given in section 6. Numerical examples are given in section 7 and the conclusion is given in section 8.

2. Coordinate Systems

The approach used here involves analyzing the equations of motion in the rotating spherical reference frame to aid in the calculation of the velocity change over a finite time interval. Starting from the well-known forms of these equations that include Coriolis and centrifugal acceleration terms, the desired change in velocity is calculated. It is then shown that a direct integration of the sum of the Coriolis and centrifugal accelerations produces a result that differs from that obtained by direct integration of the equations of motion.

Two coordinate systems are used in the analysis. These are termed the "unprimed" and "primed" coordinate systems. The systems are depicted in Fig. 1.The unprimed coordinate system is an inertial frame at rest with respect to the fixed stars. The Cartesian coordinates of this system are denoted (x, y, z). Not shown is a related unprimed spherical coordinate system (r, θ, ϕ). However, the angle ϕ of this system is depicted, and expresses the angle between the x and x' axes, and between the y and y' axes. The primed system also consists of Cartesian and spherical coordinates as shown. However, the primed system rotates about the common z, z' axes at constant angular speed $\dot{\phi} = \omega$.
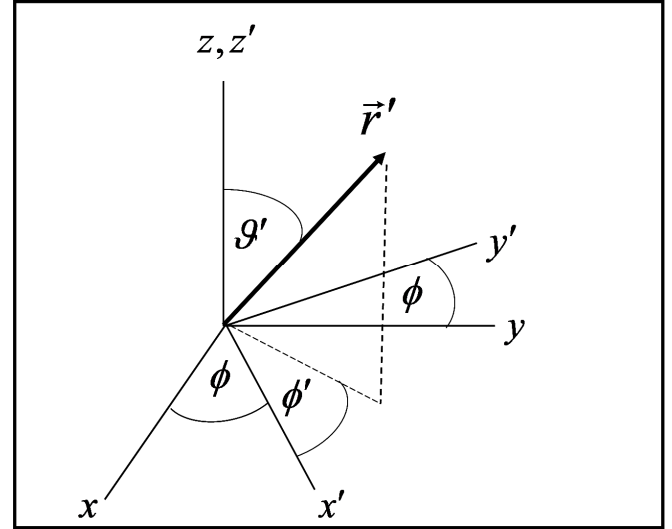

Fig 1 Primed and unprimed coordinate systems

3. Equations of Motion

In the primed coordinate system, the well-known equations of motion of an object moving on the surface with no physical tangential forces can be expressed as

$$R\ddot{\theta}' - R\dot{\phi}'^2 \sin \theta' \cos \theta' = \left[a_{COR}\right]_{\theta'} + \left[a_{CENT}\right]_{\theta'} \qquad \text{(1)}$$

and,

$$R\ddot{\phi}' \sin \theta' + 2R\dot{\theta}'\dot{\phi}' \cos \theta' = \left[a_{COR}\right]_{\phi'}. \qquad \text{(2)}$$

Here, the notations $\left[a_{COR}\right]$ and $\left[a_{CENT}\right]$ denote the Coriolis and centrifugal accelerations, respectively. It is assumed that $r' = R$, the constant radius of the sphere. The Coriolis acceleration is $\left[\vec{a}_{COR}\right] = -2\vec{\omega} \times \vec{v}'$ and the centrifugal acceleration is $\left[\vec{a}_{CENT}\right] = -\vec{\omega} \times (\vec{\omega} \times \vec{r}')$, with $\vec{v}'$ denoting velocity of the object of interest in the primed frame. These are expressed in component forms in Eq. (3) through Eq. (5)

$$[a_{COR}]_{\theta'} = 2\omega R\dot{\phi}'\sin\theta'\cos\theta', \qquad (3)$$

$$[a_{COR}]_{\phi'} = -2\omega R\dot{\theta}'\cos\theta', \qquad (4)$$

and,

$$[a_{CENT}]_{\theta'} = R\omega^2\sin\theta'\cos\theta'. \qquad (5)$$

It should be noted that $[a_{CENT}]_{\phi'}$ is zero.

4. Velocity Change Calculation

Next, expressions are developed for determining the velocity changes of the object moving on the surface over a finite time interval attributable to each of the acceleration types that appear in the problem. Students may think that these velocity changes could be computed by simply integrating the Coriolis and centrifugal accelerations over the time interval of interest. However, this is not sufficient, so the following considerations would be worthwhile addressing in class.

First, it is worthwhile defining what is meant by "velocity change" here. The velocity vector in the spherical coordinates of the primed coordinate system, assuming no radial motion, takes the form

$$[\vec{v}']_{\theta',\phi'} = R\dot{\theta}'\hat{\theta}' + R\dot{\phi}'\sin\theta'\hat{\phi}', \qquad (6)$$

with $\hat{\theta}', \hat{\phi}'$ being the usual spherical unit vectors. The velocity change of interest is taken here to be the change in the numerical value of the coefficients of the unit vectors in Eq. (6) that occur during a finite time interval. It does not include changes in the unit vectors themselves. Thus, the velocity change considered here represents the change in velocity in a given compass direction. For example, the numerical value of the coefficient of $\hat{\theta}'$ in Eq, (6) is the velocity in the northerly (or southerly) direction. As the object moves to a different latitude over the time interval of interest, the absolute meaning of "northerly" clearly changes. Nonetheless, if the object has a velocity component of 1000 miles/hour in the northerly direction at the start of the time interval, then reduces to a velocity of 800 miles/hour in the northerly direction at the end of the interval, the velocity change will be -200 miles/hour in the northerly direction, or 200 miles/hour in the southerly direction. It is not of concern here that the northerly direction points in a different direction in absolute space.

Referring to Eq. (6), it can be seen that in terms of components, the velocity changes of interest can be expressed as

$$\Delta[\vec{v}']_{\theta'} = \Delta[R\dot{\theta}'] = [R\dot{\theta}']_0^t, \qquad (7)$$

and,

$$\Delta[\vec{v}']_{\phi'} = \Delta[R\dot{\phi}'\sin\theta'] = [R\dot{\phi}'\sin\theta']_0^t. \qquad (8)$$

Here, Δ has the usual meaning of "change," and the "*0*" and "*t*" notations on the right-hand sides of the final brackets of these equations indicate the time interval of interest. Of course the lower limit need not be zero, but that is the case of interest here, and there is no loss in generality in restricting the lower limit to be zero.

The velocity changes of Eq. (7) and Eq. (8) can be re-expressed using the equations of motion as given by Eq, (1) and Eq.(2). Determining the velocity change in the θ' direction initially involves simply rearranging Eq. (1) to isolate the $R\ddot{\theta}'$ term on the left-hand side and integrating over the time interval $(0, t)$, giving

$$\int_0^t R\ddot{\theta}'\, dt = \int_0^t R\dot{\phi}'^2 \sin\theta' \cos\theta'\, dt + \int_0^t [a_{COR}]_{\theta'}\, dt + \int_0^t [a_{CENT}]_{\theta'}\, dt . \quad \text{(9)}$$

Carrying out the integral on the left-hand-side of Eq. (9) and comparing with Eq. (7) gives

$$[R\dot{\theta}']_0^t = \Delta[\vec{v}']_{\theta'} = \int_0^t R\dot{\phi}'^2 \sin\theta' \cos\theta'\, dt + \int_0^t [a_{COR}]_{\theta'}\, dt + \int_0^t [a_{CENT}]_{\theta'}\, dt. \quad \text{(10)}$$

It is immediately apparent from Eq.(10) that the velocity change $\Delta[\vec{v}']_{\theta'}$ cannot be determined simply by summing the time integrals of the Coriolis and centrifugal accelerations, since an additional term has appeared. This term arises from the second term on the left-hand-side of Eq. (1).

Determining the velocity change in the ϕ' direction involves using Eq.(2). The term $R\ddot{\phi}'\sin\theta'$ is first isolated on the left-hand-side, and again integrating both sides of the resulting equation over the interval $(0, t)$, gives

$$\int_0^t R\ddot{\phi}' \sin\theta'\, dt = -\int_0^t 2R\dot{\theta}'\dot{\phi}' \cos\theta'\, dt + \int_0^t [a_{COR}]_{\phi'}\, dt . \quad \text{(11)}$$

It is next useful to apply integration-by-parts to the integral on the left-hand-side of Eq. (11), as shown in Eq. (12)

$$\int_0^t R\ddot{\phi}' \sin\theta'\, dt = [R\dot{\phi}' \sin\theta']_0^t - \int_0^t R\dot{\phi}'\dot{\theta}' \cos\theta'\, dt \cdot \quad \text{(12)}$$

It can be seen that the first term on the right-hand-side of Eq. (12) is precisely the desired velocity change in the ϕ' direction as expressed by Eq.(8). Thus, substituting the right-hand-side of Eq. (12) for the left-hand-side of Eq. (11) and rearranging terms gives

$$\left[R\, \dot{\phi}' \sin \theta' \right]_0^t = -\int_0^t R\, \dot{\theta}'\dot{\phi}' \cos \theta'\, dt + \int_0^t \left[a_{COR} \right]_{\phi'} dt \ . \tag{13}$$

Again, comparing the left-hand-side of Eq. (13) with Eq. (8) gives,

$$\Delta \left[\vec{v}' \right]_{\phi'} = -\int_0^t R\, \dot{\theta}'\dot{\phi}' \cos \theta'\, dt + \int_0^t \left[a_{COR} \right]_{\phi'} dt \ . \tag{14}$$

Again, keeping in mind that the centrifugal contribution in the ϕ' direction is zero, it is immediately apparent from Eq.(14) that the time integral of Coriolis and centrifugal terms alone is insufficient for computing the velocity change $\Delta \left[\vec{v}' \right]_{\phi'}$, since once again another term has appeared. The new term arises from both the first and second terms on the left-hand-side of Eq. (2).

Introducing some new notation into Eq. (10) and Eq, (14) gives for the desired velocity changes

$$\left[\Delta \vec{v}' \right]_{\theta'} = \int_0^t \left[a_{COR} \right]_{\theta'} dt + \int_0^t \left[a_{CENT} \right]_{\theta'} dt + \int_0^t \left[a_{KIN} \right]_{\theta'} dt , \tag{15}$$

and,

$$\left[\Delta \vec{v}' \right]_{\phi'} = \int_0^t \left[a_{COR} \right]_{\phi'} dt + \int_0^t \left[a_{KIN} \right]_{\phi'} dt \ . \tag{16}$$

Here the notation $\left[a_{KIN} \right]$ is introduced as a way to allow convenient reference to the terms that appear in the velocity change calculations that are neither Coriolis nor centrifugal accelerations, with the subscript intended to mean "kinematic." The term kinematic is used because these terms appear purely due to describing the motion in a spherical reference frame. The components of the kinematic acceleration are given by

$$\left[a_{KIN} \right]_{\theta'} = R\, \dot{\phi}'^2 \sin\theta' \cos\theta', \tag{17}$$

and

$$\left[a_{KIN} \right]_{\phi'} = -R\, \dot{\theta}'\,\dot{\phi}' \cos\theta' . \tag{18}$$

One aspect of the kinematical components that distinguishes them from the Coriolis and centrifugal components is that they do not depend explicitly on the angular velocity of rotation, but only implicitly through their dependence on the coordinates and their time derivatives.

5. Discussion

To understand why integrating the sum of the Coriolis and centrifugal accelerations does not produce the true velocity change as seen in the rotating frame, it is helpful to consider first an object at rest in the unprimed, or absolute rest, frame. Suppose further that such an object is positioned at some latitude between the equator and the northern pole, and that the object in question is in contact with the surface of the sphere. Bearing in mind that the contact point is assumed to be frictionless, the object will remain perpetually motionless in the inertial frame, with the gravitational force and the normal force of the surface on the object exactly canceling. Since the object is at rest and is unaccelerated in the unprimed frame, it follows that in the primed frame $\dot{\vartheta}' = 0$ and $\dot{\phi}' = -\omega$. That is, in the rotating frame the object is seen to be moving in the direction opposite to that of the surface and with a rotational speed equal in magnitude to that of the surface, but oppositely directed.

Referring now to Eq. (4), and also recalling that $\left[a_{CENT}\right]_{\phi'}$ is zero as noted following Eq. (5), it is seen that the vanishing of $\dot{\vartheta}'$ guarantees that the contributions of the Coriolis and centrifugal accelerations to the acceleration component $\left[a\right]_{\phi'}$ in this example is zero. The kinematic contribution as given by Eq. (18) is also seen to be zero. Thus, there is zero net acceleration in the ϕ' direction. This is not surprising, since the object in question is

stationary in the absolute inertial frame, so it makes sense that its acceleration in the rotating frame would vanish. However, in the θ' direction the net contribution to the acceleration due to the Coriolis and centrifugal accelerations alone is not zero. This can be seen by setting $\dot{\phi}'$ equal to $-\omega$ in Eq. (3) and adding the resulting Coriolis acceleration to the centrifugal acceleration determined by Eq. (5), giving

$$\left[a_{COR} + a_{CENT}\right]_{\theta'} = -R\omega^2 \sin\theta' \cos\theta'.$$
(19)

This acceleration in the θ' direction (directed away from the equator), which is nonzero for all test locations except the equator and the poles, conflicts with the known motionlessness as seen from the inertial, or unprimed, frame. This difficulty is resolved if the kinematic contribution, as given by Eq. (17), is added to the result shown in Eq. (19). Again setting $\dot{\phi}' = -\omega$ in Eq. (17) gives for the kinematic contribution

$$\left[a_{KIN}\right]_{\theta'} = R\omega^2 \sin\theta' \cos\theta'.$$
(20)

Including the kinematic contribution, that is, adding the results given by Eq. (19) and Eq. (20) together, gives a net zero acceleration in the θ' direction, in agreement with the known object behavior in the inertial frame. The only way to reconcile the motionlessness in the inertial frame with the behavior in the θ' direction of the

noninertial frame is through the inclusion of the kinematic contribution.

6. Example Problem and Analytical Solution

A specific example will next be considered, and its exact analytical solution presented. The problem is illustrated in Fig. 2.
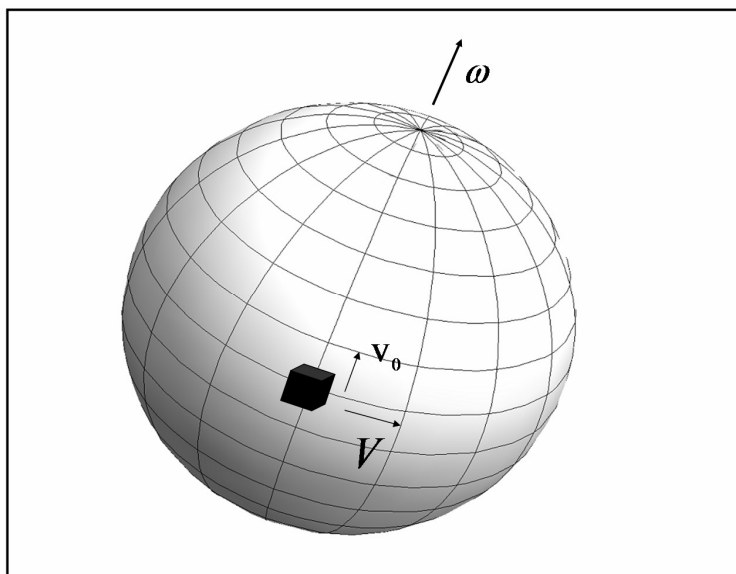

Fig 2 A sphere of radius R rotates uniformly at angular speed ω.

The block shown is in frictionless contact with the surface of the sphere of radius R. The sphere is rotating at constant angular speed ω, and the block is assumed to be constrained to remain on the surface so that the radial speed of the object is always zero. The sphere is assumed to have properties approximating those of the Earth and, as such, the pole appearing at the top of the illustration is taken to define "north," while the direction of rotation is taken to be from the "west"

and toward the "east." The velocities V and v_0 are the initial velocity components as seen in the unprimed, or inertial, frame of Fig.1. At $t = 0$ the block is located at the equator, and appears to be motionless in the east-west direction from the perspective of the rotating frame. Thus, initially, $V = R\omega$. The block is seen to have the same initial northward speed v_0 in both the primed and unprimed coordinate systems.

The initial conditions to be satisfied by the solutions of Eq.(1) and Eq. (2) are

$$(\theta', \phi')_{t=0} = (\pi/2, 0), \ \dot{\theta}'_{t=0} = -v_0/R, \text{ and } \dot{\phi}' = 0.$$

The methods of Great Circle analysis [2] are effective and straightforward for obtaining the solutions to this problem in the unprimed frame.

And the solutions in the primed frame can be obtained straightforwardly from the solutions in the primed frame using appropriate rotation matrices. In summary, when an object is given an initial velocity at any point on the surface of the sphere, from the external inertial frame the resulting motion can be described as that of an object executing uniform circular motion about a

Great Circle. In the present case, the object moves along the Great Circle at the constant speed $\sqrt{v_0^2 + V^2}$. The Great Circle is located in a plane that is tilted with respect to the plane of the equator at by the tilt angle $\arctan\left(\dfrac{v_0}{V}\right)$.

The tilt angle is taken about the x axis of Fig. 1, and is rotated from the +y axis toward the –y axis.

Transforming the solutions of Eq.(1) and Eq.(2) obtained from the Great Circle methodology subject to the given initial conditions into the primed frame produces the results that are presented in Eq. (21) and Eq, (22)

$$\theta'(t) = \arccos\left[\frac{v_0}{\sqrt{v_0^2 + V^2}}\sin\left(\frac{t\sqrt{v_0^2 + V^2}}{R}\right)\right], \tag{21}$$

and

$$\phi'(t) = \arctan\left[\frac{V}{\sqrt{v_0^2 + V^2}}\tan\left(\frac{t\sqrt{v_0^2 + V^2}}{R}\right)\right] - \omega t. \tag{22}$$

Here again, $V = R\omega$. It is straightforward to verify these solutions satisfy Eq. (1) and Eq. (2) by direct substitution. Verifying that all four initial conditions are satisfied is also straightforward. Students can derive these solutions as an assignment or they can be derived in class. Carrying the calculations through is not difficult using a symbol manipulator such as Maple™ or Mathematica™. Solution verification is also straightforward using this kind of software.

Once these solutions have been presented, it would be worthwhile to point out to the students the advantage of such analytic representations relative to a purely numerical solution [1]. Numerical solutions are subject to error due to improperly chosen step size or insufficient numbers of digits used to represent the numbers being manipulated. There is even a possibility of bugs in the numerical software. These concerns are allayed with an available analytical solution.

Calculations based on applying the formulas are also possible that could only be performed by trial and error using a purely numerical approach.

7. NUMERICAL CALCULATIONS

Two numerical examples are considered. In the first, the block has the initial northerly speed $V_0 = 50$ miles/hour. This is perhaps a realistic speed that may appear in the movement of the atmosphere. However, much of the interesting physics is only seen when the initial speed V_0 has an extreme value. Thus, in the second example the block has an initial speed of $V_0 = 5000$ miles/hour.

Considering the case where $V_0 = 50$ miles/hour, it should first be mentioned that the object will

reach a maximum northerly distance from the equator, reverse direction, then eventually return to the equator and will then proceed to move into the southern hemisphere. One calculation of interest is the maximum northerly distance from the equator reached by the object. At this position $\dot{\theta}' = 0$. Differentiating Eq. (21) with respect to time determines $\dot{\theta}'$, and the first root of this expression after $t = 0$ determines the first time when the northerly motion turns toward the south. The maximum northerly displacement is then determined from the expression $R\left(\pi/_2 - \theta'\right)$, where θ' is computed using Eq. (21) evaluated at the just-determined time where $\dot{\theta}' = 0$. The maximum northerly displacement produced by this procedure for the current example is approximately 190.84 miles.

Since the object then reverses its direction of motion in the θ' direction, it is evident that the initial northerly speed of 50 miles/hour has been reduced to zero by the three accelerations operating in the θ' direction. Also of interest is the amount of velocity reduction contributed by each of these accelerations. This is determined by separately evaluating each of the three integrals appearing in Eq. (15), again using for the upper limit the just-determined time where $\dot{\theta}' = 0$. The results are $\left[\Delta V_{COR}\right]_{\theta'}$ = -0.151429 miles/hour, $\left[\Delta V_{CENT}\right]_{\theta'}$ = -49.8484 miles/hour, and $\left[\Delta V_{KIN}\right]_{\theta'}$ = -0.000138051 miles/hour, where the subscripts on the velocity-change symbols correspond to the subscript conventions for each acceleration appearing in Eq. (15). It is evident that the kinematic contribution is negligible in this case, which is one reason an extreme example is also considered.

One final calculation of interest in the 50 miles/hour case is the maximum easterly speed reached by the object due to each of the two accelerations acting in that direction, and the contributions to that speed change by each acceleration component. The maximum easterly speed is obtained by evaluating the integrals appearing in Eq. (16). The upper time limit of these integrals is determined by finding the location of the first maximum of the function $R\dot{\phi}'\sin\theta'$ after $t = 0$. It is found that this first maximum occurs at the same time at which the maximum northerly displacement is reached, that is, when $\dot{\theta}' = 0$. To understand why this is so, it is helpful first to realize that when the function $R\dot{\phi}'\sin\theta'$ is differentiated with respect to time, one of the two resulting terms contains a factor of $\dot{\theta}'$ and the other term contains a factor of $\ddot{\phi}'$. By rearranging Eq. (2), $\ddot{\phi}'$ can be isolated on the left-hand side. Doing this, it is seen that all terms on the right hand side of the resulting equation contain a factor of $\dot{\theta}'$. It follows that the derivative of $R\dot{\phi}'\sin\theta'$ with respect to time vanishes when $\dot{\theta}'$ is zero.

The results of carrying out the integrals in Eq. (16) are that the maximum easterly speed obtained by the object is 2.38461 miles/hour. The separate contributions to the result are $\left[\Delta V_{COR}\right]_{\phi'}$ = 2.38325 miles/hour and $\left[\Delta V_{KIN}\right]_{\phi'}$ = 0.00135752 miles/hour.

Although the example involving $V_0 = 50$ miles/hour is interesting since it considers a speed that is perhaps comparable to atmospheric winds, that example does not reveal all the interesting physics of the problem. We thus consider now a second example where $V_0 = 5000$ miles/hour. This example differs substantially from the 50

mile/hour case. Since the initial velocity is so great, rather than computing the maximum northerly displacement it is more interesting to compute the distance of closest approach to the northern pole. Considering the large starting speed, it might be supposed that the object would closely approach the pole. It may be surprising then to learn that the distance of closest approach in this case is 825.82 miles, still a considerable distance away.

As with the first example, it is also interesting to compute how much velocity change is contributed by each of the three accelerations in reducing the initial northerly velocity to zero. The results are

$$\left[\Delta \mathrm{V}_{COR}\right]_{\theta'} = -742.85 \text{ miles/hour,}$$

$$\left[\Delta \mathrm{V}_{CENT}\right]_{\theta'} = -115.28 \text{ miles/hour, and}$$

$$\left[\Delta \mathrm{V}_{KIN}\right]_{\theta'} = -4141.87 \text{ miles/hour. Thus unlike}$$

the previous example where the kinematic contribution was negligibly small, in the current case the kinematic contribution is rather dominant.

The maximum easterly speed and the contributions of each of the two accelerations that involved in attaining it are also of interest. The maximum easterly speed is 4893.82 miles/hour. The contributions of the individual accelerations are

$$\left[\Delta \mathrm{V}_{COR}\right]_{\phi'} = 1665.06 \text{ miles/hour and}$$

$$\left[\Delta \mathrm{V}_{KIN}\right]_{\phi'} = 3228.76 \text{ miles/hour. So again}$$

unlike the previous example, the kinematic contribution dominates, though not as significantly as with the northerly velocity change.

8. CONCLUSION

The problem of computing the components of the velocity change in the rotating frame of an object moving on the surface of a rotating sphere under conditions of no physical tangential forces was solved exactly. In the rotating frame the well-known Coriolis and centrifugal fictitious accelerations appear. However, it was shown that

integrating only these two acceleration terms over a finite time interval does not yield the correct result for the determination of the velocity change. The additional terms that must be included in the calculation were herein termed the "kinematic" acceleration for the purpose of easy reference. In the two numerical examples that were considered, it was found that the kinematic contribution is negligibly small when an initial velocity comparable to atmospheric winds was considered, but was found to be dominant when an extremely high initial velocity was considered. Such an extremely high atmospheric velocity may be realistic for some exoplanet that has a substantially thinner atmosphere than that of the Earth. Even within the solar system, very high wind speeds have been observed. For example, a wind speed of approximately 1300 miles/hour has been seen on Neptune [11].

It should be emphasized that the concept of kinematic acceleration introduced here is not some "new" acceleration term that has somehow been missed by previous workers in the area of spherical rotating reference frames. The physics of the problem is completely contained in the equations of motion as given in Eq.(1) and Eq. (2). These equations have been known at least since the time of Coriolis. However, if one is interested in the calculation of the change of velocity over a finite time interval, and one then asks the question, "How much of the velocity change is due to each acceleration component (?)," one may very well be surprised to find that the Coriolis and centrifugal contributions sum up to less than 100% of the change. One is then likely to ask, "Where does the rest of the velocity change come from?" It is in answering this last question where the concept of the kinematic acceleration is useful.

It is hoped that the results presented here will be of use to those who teach subjects related to rotating frames. The velocity change calculation of interest and the example problem considered were capable of exact solution using relatively

elementary methods. Such exactly solvable problems are rare.

References:

[1] A. Amengual, "Noninertial trajectories on a fast rotating planet," Am. J. Phys. **68** 1106-1108 (2000).

[2] D. H. McIntyre, "Using great circles to understand motion on a rotating sphere," Am. J. Phys. **68** 1097-1105 (2000).

[3] Warren Weckesser ,"A ball rolling on a freely spinning turntable" **,** Am. J. Phys. **65**, 736 (1997).

[4] Martin S. Tiersten and Harry Soodak , "Dropped objects and other motions relative to the noninertial earth", Am. J. Phys. **68** , 129 (2000) .

[5] Houston C. Saunderson, "Equations of motion and ballistic paths of volcanic ejecta", Computers & Geosciences **34**, 802 (2008).

[6] A. P. French, ''The Deflection of Falling Objects,'' Am. J. Phys. **52**, 199 (1984).

[7] J. M. Potgieter, ''An exact solution for the horizontal deflection of a falling object,'' Am. J. Phys. **51**, 257–258 (1983).

[8] E. Belorizky and J. Sivardie`re, ''Comments on the horizontal deflection of a falling object,'' Am. J. Phys. **55**, 1103–1104 (1987).

[9] E. A. Desloge, ''Further comments on the horizontal deflection of a fallingobject,'' Am. J. Phys. **57**, 282–284 (1989).

[10] M. Kugler, "Motion in noninertial systems: Theory and demonstrations", Am. J. Phys. **57** , 247 (1989) .

[11] V. E. Suomi, S. S. Limaye, and D. R. Johnson, "High Winds of Neptune: A possible mechanism," Science **251** 929–932 (1991).

Doppler Shift of the de Broglie Waves- Some New Results from Very Old Concepts

Sanchari De and Somenath Chakrabarty

Department of Physics, Visva-Bharati, Santiniketan 731 235, India

somenath.chakrabarty@visva-bharati.ac.in

Abstract

The Doppler shift of de Broglie wave is obtained for fermions and massive bosons using the conventional form of Lorentz transformations for momentum and energy of the particles. A formalism is developed to obtain the variation of wave length for de Broglie waves with temperature for individual particles using the classic idea of Wien in a many body Fermi gas or massive Bose gas.

1 Introduction

It is well known that the pitch of an audible acoustic wave appears to change if there is a relative motion between the source and the observer. Such apparent change in frequency of sound waves when there is a non-zero relative velocity is known as the Doppler effect in the case of acoustics. Same kind of physical effect is also been observed in the case of optics with an apparent change in wavelength or color of the light. With simple theoretical calculation one can show that the effect is common to all kinds of travelling waves. However, to make appreciable change in frequency or wavelength for light waves the relative velocity must be a considerable fraction of the velocity of light. Since the speed of light is extremely high compared to the speed of any terrestrial object, it is difficult to detect any measurable or observable change in wavelength or color of the emitted light from any source having relative motion with respect to the observer. Whereas many of the stellar objects are moving with very high ve-

locity, therefore wavelength of light emitted from these heavenly bodies, moving either towards or away from the earth show measurable amount of blue or redshift respectively in the spectral lines. The possibility of shift in the position of a spectral line due to relative motion of the source and the observer was first pointed out by Doppler in the year 1842. From the observed red shift and blue shift of spectral lines, it has been reported that the stars like Sirius, Caster, Regulus are moving away from the earth, whereas, the stars like Arcturus, Vega and α Cygni are moving towards the earth. An extremely interesting application of the Doppler effect is to the discovery of spectroscopic binaries. The Doppler principle has also been applied to determine the nature of Saturn's ring.

Since the effect of relative motion of source and observer on apparent change in frequency or wavelength is common to all kinds of waves. We expect that the de Broglie waves will also be Doppler shifted if there is a relative motion between the emitter and the detector (see [1] for a very nice discussion). In this article, based on three old classic pieces of discoveries- the Doppler effect in the year 1842, the Wien's displacement law in the year 1893 and the matter wave or the de Broglie wave in the year 1923 [2, 3, 4], we shall study the Doppler shift of de Broglie waves associated with fermions or bosons inside many body Fermi system or Bose system respectively. In our investigation, instead of conventional photon or phonon gas, we have considered bosons of non-zero mass. Then using the classic idea of Wien we shall develop a formalism to express the variation of de

Broglie wavelength for the individual particles with the temperature of the system for both fermions and bosons. The relations may be called as the modified form of the Wien's displacement law for black body Fermi gas or Bose gas. To the best of our knowledge this problem has not been addressed before.

2 Doppler Shift of de Broglie Waves

We consider a many body quantum system consisting of either fermions or bosons. Then without the loss of generality, we may assume that just like a black body system of electromagnetic waves or photon gas, the system is essentially a gas of a large number of de Broglie waves of fermions or bosons. Hence we may call the system as a black body Fermi gas or Bose gas. We have further assumed that the collisions among the particles is elastic in nature. To obtain the change in wavelength for de Broglie waves due to Doppler effect, we start with the well known form of Lorentz transformations of particle momentum and energy. We assume two frame of references, S, the rest frame and the frame S' is moving with respect to S with a uniform velocity V along x-direction. We further assume that the motion of the particle is on $x - y$ plane. Then we have from the standard text book results [5], the Lorentz transformation for the x-component of parti-

cle momentum

$$p'_x = \gamma \left(p_x - \frac{VE}{c^2} \right) \ \text{ with } \ \gamma = \left(1 - \frac{V^2}{c^2} \right)^{-1/2} \tag{1}$$

where E is the energy of the particle in S-frame and c is the velocity of light. If θ and θ' are the angles subtended by the particle momenta $\vec{p}$ and $\vec{p'}$ with the x-direction in S and S' frames respectively, then we have from eqn.(1)

$$p' \cos \theta' = \gamma \left(p \cos \theta - \frac{VE}{c^2} \right) \tag{2}$$

and since $p'_y = p_y$, hence we can write $p' \sin \theta' = p \sin \theta$.

Now defining the de Broglie wavelengths in these two frames as $\lambda = h/p$ and $\lambda' = h/p'$, and using $E = (p^2 c^2 + E_0^2)^{1/2}$, the particle energy in S frame and a similar expression for E' in S' frame, with $E_0 = m_0 c^2$, the rest mass energy, we have

$$\frac{\lambda}{\lambda'} \cos \theta' = \gamma \left[\cos \theta - \frac{V}{c} \left\{ 1 + \left(\frac{\lambda}{\lambda_c} \right)^2 \right\}^{1/2} \right] \tag{3}$$

where $\lambda_c = h/m_0 c$, the Compton wavelength. Then it can very easily be shown that the aberration is given by

$$\tan \theta' = \frac{\sin \theta}{\gamma \left[\cos \theta - \frac{V}{c} \left\{ 1 + \left(\frac{\lambda}{\lambda_c} \right)^2 \right\}^{1/2} \right]} \tag{4}$$

Now it is a matter of simple algebra to verify that for the mass-less case when $\lambda_c = \infty$, the usual results for electromagnetic waves or photons can be obtained from the eqns.(3) and (4).

To obtain the Doppler shift of the de Broglie waves for the particles it is more convenient to start from the Lorentz transformation for the particle energy, given by

$$E' = \gamma (E - V p_x) \tag{5}$$

Squaring both the sides and using the definition of de Broglie waves in both S and S' frames, we have

$$\frac{\lambda}{\lambda'} = \gamma \left[1 - \frac{2V}{c} \cos \theta \left\{ 1 + \left(\frac{\lambda}{\lambda_c} \right)^2 \right\}^{1/2} + \left(\frac{V}{c} \right)^2 \left\{ \cos^2 \theta + \left(\frac{\lambda}{\lambda_c} \right)^2 \right\} \right]^{1/2} \tag{6}$$

Again it is very easy to verify that the results for electromagnetic waves follow from here for $\lambda_c = \infty$.

It is also obvious that the transverse form

of Doppler shift with $\theta = \pi/2$ is non-vanishing in the case of matter waves and is given by

$$\frac{\lambda}{\lambda'} = \gamma \left[1 + \left(\frac{V}{c} \right)^2 \left(\frac{\lambda}{\lambda_c} \right)^2 \right]^{1/2} \qquad (7)$$

3 Variation of de Broglie Wavelength with Temperature

To obtain the variation of de Broglie wavelength with temperature, we consider either a Fermi gas or a Bose gas of non-zero mass in an enclosure, just like the black body chamber of a photon gas. For the sake of simplicity the enclosure is assumed to be spherical in nature. Further the wall of the enclosure is assumed to be a perfect reflector and moving outward adiabatically with a velocity V, where V is small enough compared to the velocity of light. The moving wall of the enclosure may be treated as S' frame, whereas the S frame is at rest inside the enclosure with a fictitious observer sitting there. The tangential plane at some arbitrary point on the outer surface of the wall is assumed to be in the $y - z$ plane. Then the normal drawn from the centre to this point of intersection is the x-direction. The particle which is hitting the wall at this point of intersection is as before assumed to be moving in $x - y$ plane. Then for a de Broglie wave of wavelength λ, the point of intersection on the moving wall at which it is hitting is equivalent to an observer moving away from the source, which is

radially outward along x-direction. As a consequence the received de Broglie wave at the moving wall will be red shifted and is given by

$$\frac{\lambda}{\lambda'} = \left[1 - \frac{2V}{c} \frac{\lambda}{\lambda_c} \cos \theta \right]^{1/2} \qquad (8)$$

where we have neglected the term $(V/c)^2$ and assumed that $\lambda \gg \lambda_c$ in the non-relativistic approximation. When the particle is reflected back from the point of incidence, since the wall is moving outward, it is equivalent to the emission from a source moving away from the observer. Therefore in this case also the de Broglie wave of the particle will be red shifted as observed from S frame. Combining these two effects, the relation between the final red shifted wavelength to that of the original one is given by

$$\frac{\lambda''}{\lambda} = \frac{\left[1 + \frac{2V}{c} \frac{\lambda''}{\lambda_c} \cos \theta \right]^{1/2}}{\left[1 - \frac{2V}{c} \frac{\lambda}{\lambda_c} \cos \theta \right]^{1/2}} \qquad (9)$$

Since $V/c \ll 1$, we have approximately

$$\frac{\lambda''}{\lambda} \approx \frac{\left[1 + \frac{V}{c} \frac{\lambda}{\lambda_c} \cos \theta \right]}{\left[1 - \frac{V}{c} \frac{\lambda}{\lambda_c} \cos \theta \right]} \qquad (10)$$

If we assume that the amount of final red shift is infinitesimal, the above relation may further be approximated to

$$\frac{\lambda''}{\lambda} \approx 1 + \frac{2V}{c} \frac{\lambda}{\lambda_c} \cos \theta \qquad (11)$$

Writing the final red shifted wave length $\lambda'' = \lambda + d\lambda$, we have the resultant infinitesimal change in wave length

$$d\lambda = \frac{2V}{c} \frac{\lambda^2}{\lambda_c} \cos \theta \qquad (12)$$

To eliminate the arbitrary angle of incidence θ, we consider multiple reflection of de Broglie waves from the inner wall of the enclosure. For spherical geometrical structure, with radius r, a de Broglie wave travels a distance $2r\cos\theta$ between two successive collisions. Therefore the number of reflections per unit time is $v/2r\cos\theta$. Hence the change in wavelength per unit time is

$$d\lambda = \frac{V}{c}\frac{\lambda^2}{\lambda_c}\frac{dr}{r} \qquad (13)$$

where we have assumed that the particle travels δr distance in unit time and in the limiting case it is dr.

Now from the first law of thermodynamics we have for an adiabatic change, $dQ = dU + PdV_0 = 0$. Hence we know for a non-relativistic Fermi or Bose gas $PV_0^{5/3} =$ constant.

Now with the standard results from the textbook on statistical mechanics [6], the energy density for free Fermi gas or Bose gas is given by

$$\epsilon = \frac{3}{2}\frac{kT}{\lambda_0^3}f_{5/2}(z) \quad \text{and} \quad \epsilon = \frac{3}{2}\frac{kT}{\lambda_0^3}g_{5/2}(z) \quad \text{respectively,} \qquad (14)$$

$$\text{where} \quad f_{5/2}(z) = \sum_{l=1}^{\infty}(-1)^{l-1}\frac{z^l}{l^{5/2}}, \quad g_{5/2}(z) = \sum_{l=1}^{\infty}\frac{z^l}{l^{5/2}}, \quad \lambda_0 = \frac{\hbar}{(2\pi mkT)^{1/2}}$$

$$\text{and} \quad z = \exp\left(\frac{\mu}{kT}\right) \qquad (15)$$

the fugacity, with μ, the chemical potential of the constituents. The functions $f_\nu(z)$ and $g_\nu(z)$ are the Fermi function and Bose function respectively.

Since for a many body Fermi system, whether it is electron gas in a piece of metal or inside white dwarfs or neutron matter inside neutron stars, the chemical potential μ is always non-zero. Therefore it is quite obvious that from eqns.(14) and (15) an analytical expression for energy density for a Fermi gas can not be obtained. We therefore approximate the Fermi gas by Boltzmann statistics.

Then it is very easy to show that

$$P = \frac{2}{3}\epsilon \quad \text{and} \quad P \propto \exp\left(\frac{\mu}{kT}\right)T^{5/2}$$

Hence from the adiabatic relation between pressure and volume, we have

$$\exp\left(\frac{2\mu}{5kT}\right)Tr^2 = \quad \text{constant} \qquad (16)$$

where we have used $V_0 = 4\pi r^3/3$, the volume of the enclosure at some instant. Taking log

of both the sides and then differentiating all the terms and finally using eqn.(13), we have

$$\left(-\frac{2\mu}{5k}\frac{1}{T^2} + \frac{1}{T}\right)dT = -2\frac{dr}{r} = -2\frac{c}{V}\frac{\lambda_c}{\lambda}\frac{d\lambda}{\lambda} \tag{17}$$

Now integrating and rearranging the terms and finally redefining λ and T as λ^* and T^*, we have

$$\frac{1}{\lambda^*} - \frac{1}{T^*} = \ln\left(\frac{T}{T_0}\right) \tag{18}$$

where

$$\frac{1}{\lambda^*} = \frac{2\lambda_c c}{V}\frac{1}{\lambda}, \quad \frac{1}{T^*} = \frac{2\mu}{5k}\frac{1}{T} \quad \text{and} \quad T_0 \text{ is a positive constant}$$

The above equation (eqn.(18)) looks like the equation for a thin lens, where the right hand side is the inverse of focal length. Now it is well known that at high temperature a Fermi gas behaves like a Boltzmann gas and then the de Broglie wavelengths for the particles become infinitely large. Therefore the right hand side must be negative, i.e., $T < T_0$. Hence we can say that eqn.(18) may be compared with the equation for the convex lens. The temperature at which a fermion behaves like a classical particle can be obtained from the numerical solution of the equation $T^* \ln(T/T_0) + 1 = 0$. At this temperature, the de Broglie wavelength becomes infinitely large and above this temperature eqn.(18) does not hold. The system behaves classically. As $T \longrightarrow 0$, the magnitude of the second term on the left hand side of eqn.(18) becomes infinitely large much before the right hand side goes to $-\infty$. Therefore we may conclude that as temperature decreases, the de Broglie wavelength also decreases. Which means that the quantum me-chanical effect becomes more and more important. In the extreme case, at $T \longrightarrow 0$, the Wave length tends to zero. If one compares eqn.(18) with the equation for a convex lens, then it is quite obvious that $\lambda = \infty$ corresponds to the object on the first focal plane of the convex lens in the object space, for which the real image is formed at infinity. In the case of a Fermi gas the temperature at which this happens, the de Broglie wavelength becomes infinitely large. This is also the limiting temperature separating the temperature space into a quantum zone and a classical zone. Now it is well known that beyond the first focal plane away from the convex lens, the images are always real, which in the present scenario corresponds to classical picture. In the case of a convex lens the object space between the focal plane and the lens always produce virtual images. Same kind of picture is true here also. The temperature zone between the upper critical value and $T \longrightarrow 0$ is the quantum mechanical region. So the quantum mechanical region of

temperature in the present scenario corresponds to the object space producing virtual images in the case of a convex lens. There is perhaps nothing wrong in such comparison of quantum mechanical temperature zone with the object space produce virtual images. In the quantum mechanical zone, because of uncertainty principle the exact location of the particle can not be predicted, only the probability of existence at a point can be obtained from the wave function of the particle. Therefore grossly speaking, a cloudy picture will be observed instead of a real location of the particle.

We next consider a massive Bose system. It may be a $\pi^+ - \pi^-$ matter or a neutral pion matter or even a system of extremely rarefied cold atoms. Since for these bosonic systems there is as such no conserved quantum number, the chemical potential for the constituents are exactly zero. Then we have from eqn.(18) (Now in the case of bosons, the chemical potential $\mu = 0$, therefore energy density can be obtained from the second expression as given by eqn.(14). The series $g_{5/2}(1)$ can be expressed in terms of known Zeta-function)

$$\frac{1}{\lambda} = \frac{V}{2\lambda_c c} \ln\left(\frac{T}{T_0}\right) \ \text{ or } \ \lambda \ln\left(\frac{T}{T_0}\right) = \text{ constant}$$
(19)

This is again the form of Wien's displacement law for the massive Bos gas. From the nature of the above equations and the properties of massive bosons, one can infer that T_0 is the minimum value of temperature for a Bose system at which $\lambda = \infty$. In this crude model calculation we may say that this is the tempera-

ture for Bose condensation of the gas. Therefore, T_0 in eqn.(18) and eqn.(19) are carrying quite different physical meaning. Since in the condensed phase all the bosons occupy the same quantum state, the spatial coherence length will be large enough in the atomic scale. In this simple model it is reflected by the extremely large value of de Broglie wavelength, which is large enough in the quantum scale. Then as the temperature increases, the system becomes more and more incoherent because of the randomness, and at very high temperature the system becomes a classical gas. Of course with this crude model calculation this can not be shown. For mass-less bosons, i.e. with $m = 0$, since $\lambda_c = \infty$, the above equation can not predict the condensation temperature. Which is already known for photon gas and phonon gas.

4 Conclusions

It is therefore quite surprising that based on three very old classic pieces of discoveries- the Doppler effect in the year 1842, the Wien's displacement law in the year 1893 and the matter wave or the de Broglie wave in the year 1923, it is possible to predict the variation of de Broglie wavelength with temperature for individual fermions and bosons in a many particle system. It is also possible to obtain the temperature beyond which the fermionic system behaves classically, the critical temperature for Bose condensation for massive Bose gas and also one can conclude that for mass-less bosons the critical temperature of Bose condensation can not be pre-

dicted.

References

[1] Keeyung Lee, New Physics: Sae Mulli (The Korean Physical Society), **61**, 2011, 222, see also Anatoli Vankov, Annales de la Foundation, **30**, 2005, 15.

[2] Steven Weinberg, Gravitation and Cosmology Principles and Applications of the General Theory of Relativity, John Wiely & Sons, New York, 1972.

[3] M.N. Saha and B.N. Srivastava, A Treatise on Heat, The Indian Press PVT LTD, Allahabad, 1976.

[4] L.D. Landau and E.M. Lifshitz, Quantum Mechanics, Pergamon Press, London, 1959.

[5] L.D. Landau and E.M. Lifshitz, Classical Theory of Fields, Pergamon Press, London, 1959.

[6] K. Huang, Statistical Mechanics, Wiley Eastern PVT LTD, 1963.

Momentum Representation of Wave Function in Quantum Harmonic Oscillator Using Spreadsheets

Popat S. Tambade

Department of Physics

Prof. Ramkrishna More Arts, Commerce and Science College, Akurdi

Pune 411044, India.

Savitribai Phule Pune University, Pune

Email: pstam3@rediffmail.com

Abstract

In this article author have developed computer simulation using Microsoft Excel 2007® to graphically illustrate the wave functions and their momentum representations. Using this simulations wave functions in different states can be plotted. The expectation values of x and x^2 can be obtained by using the simulation. Using momentum representation <p> and <p^2> are obtained. Using the expectation values of position and momentum the uncertainty principle verified. The momentum representation is seldom used in quantum mechanics courses hence students find it difficult to understand.

Introduction

Quantum mechanics is one of the most widely taught topics on the college and university level as it has fundamental role in physics and chemistry. Quantum mechanics is technically difficult to learn because it is mathematically challenging and abstract in nature. Students constantly struggle to master the basic concepts. It is difficult for students to interpret and draw qualitative inferences from mathematics representations [1]. Fast and realistic based computer visualization tools can play key role in teaching and learning of quantum mechanics [2].

From data analysis and graphing to animation and simulations, Microsoft Excel® is a very versatile program for the researchers, teachers and students. The strong features of spreadsheet are their cell based structure and the simple interface that is easy to use for new users also. With a variety of built-in mathematical functions and excellent graphics

capabilities, the spreadsheet becomes a powerful instrument for modeling problems in quantum physics as well as in many areas of the physics. In a spreadsheet, the data manipulations are held in front of the user in a very direct and accessible manner. In addition, the spreadsheet program itself provides for screen graphics, charts, and easy-data manipulation using large number of functions, on-screen numerical and visual feedback, and fast calculations[3, 4, 5].

In quantum mechanics, the position ($\hat{x}$), and the linear momentum ($\hat{p}$) operators play very symmetrical roles as it must be obvious from the fundamental commutation relation $[\hat{x}, \hat{p}] = i\hbar$. However, this fundamental symmetry may not be apparent to many students of quantum mechanics since more emphasis is given on the coordinate representation in lectures and in textbooks. In this

study, the author has discussed an example of one-dimensional harmonic oscillator in quantum mechanics from the point of view of momentum space [6]. For this purpose, spreadsheet based simulation was developed and graphical representation of momentum space counterpart $\varphi(p)$ of coordinate space wave function $\psi(x)$ is obtained using Fourier transform. From the $\psi(x)$ and $\varphi(p)$ representations uncertainties in the position and momentum are obtained. These values found to be in agreement with the desired results. From these wave functions uncertainties in position and momentum are calculated.

1. Harmonic Oscillator

The potential energy for harmonic oscillator is

$$V(x) = \frac{1}{2}kx^2$$

The Hamiltonian is given as

$$H = -\frac{\hbar^2}{2m}\frac{d^2}{dx^2} + \frac{1}{2}kx^2$$

The Schrodinger's steady state equation for harmonic oscillator is given as

$$\frac{d^2\psi}{dx^2} + \frac{2m}{\hbar^2}\left(E - \frac{1}{2}kx^2\right)\psi = 0 \qquad \ldots(1)$$

The energy eigen values of harmonic oscillator are

$$E_n = \left(n + \frac{1}{2}\right)\hbar\omega$$

The unperturbed eigen functions are

$$\psi_n(x) = \left(\frac{1}{2^n n!\sqrt{\pi}}\right)H_n(\alpha x)e^{-\alpha^2 x^2/2} \qquad \ldots(2)$$

where n=0, 1, 2, …….

The classical limit is given as

$$x_0 = \sqrt{\frac{2E_n}{m\omega^2}} \qquad \ldots(3)$$

It is convenient to simplify Eq. (1) by introducing the dimensionless quantities. Let us introduce dimensionless variable $\xi = \alpha x$, we get

$$\frac{d^2\psi}{d\xi^2} + \left(2\varepsilon - \xi^2\right)\psi = 0 \qquad \ldots(4)$$

where $\alpha = \left(\frac{m\omega}{\hbar}\right)^{1/2}$ and $\varepsilon = \frac{E}{\hbar\omega}$.

The eigen functions are

$$\psi_n(\xi) = \left(\frac{1}{2^n n!\sqrt{\pi}}\right)^{1/2} H_n(\xi)e^{-\xi^2/2} \qquad \ldots(5)$$

where $H_n(\xi)$ are Hermite polynomials of order n. The Hermite polynomials satisfy the following recurrence relation,

$$H_{n+1}(x) = 2xH_n(x) - 2nH_{n-1}(x) \qquad \ldots(6)$$

The classical limit in terms of dimensionless variable is $\xi_0 = \sqrt{2n+1}$

The energy parameter is defined as

$$\varepsilon_n = \frac{E_n}{\hbar\omega}$$

Therefore,

$$\varepsilon_n = \left(n + \frac{1}{2}\right) \qquad \ldots(7)$$

The uncertainty is ξ is

$$\Delta\xi = \sqrt{n + \frac{1}{2}}$$

We generate the momentum wave function by Fourier transform of the coordinate-space wave function and given as [7]:

$$\Phi_n(p) = \frac{1}{\sqrt{2\pi\hbar}}\int_{-\infty}^{\infty}\psi_n(x)\,e^{-ipx/\hbar}dx \qquad \ldots(8)$$

This Fourier transform illustrates that each point in p-space is intertwined with every point in x-space, and vice versa.

Let $\eta = p/\sqrt{m\omega\hbar}$ with classical limit $\eta_0 = \sqrt{2n+1}$, we write above equation in η-space as

$$\Phi_n(\eta) = \frac{1}{\sqrt{2\pi}}\int_{-\infty}^{\infty}\psi_n(\xi)\,e^{-i\eta\xi}d\xi \qquad \ldots(9)$$

The function $\Phi(\eta)$ also satisfies the normalization equation, i.e. $\int_{-\infty}^{\infty}|\Phi_n(\eta)|^2\,d\eta = 1$

The expectation values are

$$<\eta> = \int_{-\infty}^{\infty}\eta\,|\Phi_n(\eta)|^2\,d\eta$$

$$<\eta^2> = \int_{-\infty}^{\infty}\eta^2\,|\Phi_n(\eta)|^2\,d\eta$$

The uncertainty of wave number *k* is

$$\Delta\eta = \sqrt{<\eta^2> - <\eta>^2}$$

We get $(\Delta\eta)^2 = \left(n + \dfrac{1}{2}\right)$

The product of uncertainties has value as

$$\Delta\xi\,\Delta\eta = \left(n + \frac{1}{2}\right) \text{ or } \Delta x\,\Delta p = \left(n + \frac{1}{2}\right)\hbar$$

Because of its symmetry, the harmonic oscillator is as easy to solve in momentum space as it is in position space. It gives the same results as the wave function in the position basis.
Using Microsoft excel 2007 this result is verified..

2. Organization of Spreadsheet

Using spreadsheet the wave functions are obtained from $-3\xi_0$ to $+3\xi_0$. The probability density is plotted. The uncertainty in the position is obtained. The values of η are set from $-3\eta_0$ to $+3\eta_0$. The Fourier transform is obtained. The real part of Fourier transform is

$$R(\eta) = \frac{1}{\sqrt{2\pi}} \sum_{-3\xi_0}^{3\xi_0} \psi(\xi)\cos(\eta\xi)d\xi$$

The imaginary part is

$$I(\eta) = \frac{1}{\sqrt{2\pi}} \sum_{-3\xi_0}^{3\xi_0} \psi(\xi)\sin(\eta\xi)d\xi$$

The spreadsheet developed as

B5: cell named as 'n' and it contains value of n.
B7: cell named as 'a' and it contains value of ξ_0.
D8: cell named as 'dx' and it contains value of dx obtained by formula $= 3\xi_0/400$
F7: cell named as 'dk' and it contains value of $d\eta$ obtained by formula $= 3\eta_0/400$
B28:B828: Range named as 'x' contain values of ξ by increment of $d\xi$
C28:C828: Range named as 'y' contain values of $\psi(\xi)$ which is obtained by formula

"=SQRT(1/(fact(n)*2^n*sqrt(pi())))*Her(n,x)*exp(-x^2/2)"   …(5)

E28:E828: Range named as 'k' and contain values of 'η' by the interval of $d\eta$.

The real part of Fourier transform is obtained in F28:F828. In cell F28 the formula used is
$= $ SUMPRODUCT(y, os(E27*x)) *dx /SQRT(2*pi())
The formula gives the value of $R(\eta)$ for η value in cell E28. The formula is copied up to F828.
The imaginary part of Fourier transform is obtained in G28:G828. The formula used in the range is
$= $ SUMPRODUCT(y, sin(E27*x)) *dx /SQRT(2*pi())
The formula gives the value of $I(\eta)$ for η value in cell E28. The formula is copied up to G828.
H28:H828 contain value of $|\phi(\eta)|^2$ and the range is named as D.
To obtain uncertainty product values the formulas used are listed in Table 1.

Table 1: List of formulas used in different cells of worksheet

cell	Value	Formula in cell
H6	$<\xi>$	= SUMPRODUCT(x,y^2*dx)
H7	$<\xi^2>$	= SUMPRODUCT(x^2,y^2*dx)
H8	$\Delta\xi$	=SQRT(H7 – H6^2)
J6	$<\eta>$	= SUMPRODUCT(k,D*dk)
J7	$<\eta^2>$	= SUMPRODUCT(k^2,D*dk)
J8	$\Delta\eta$	=SQRT(J7 – J6^2)
J9	$\Delta\eta\,\Delta\xi$	=H8*J8
D9	$\sum |\psi(\xi)|^2\,d\xi$	=SUMPRODUCT(y^2*dx)

F9	$\sum |\Phi(\eta)|^2 \, d\eta$	=SUMPRODUCT(D*dk)

To find value of Hermite polynomials an User Define function Her(n,x) was built up using VBA and recurrence relation given in Eq. (6) is used to find values of higher order polynomials.

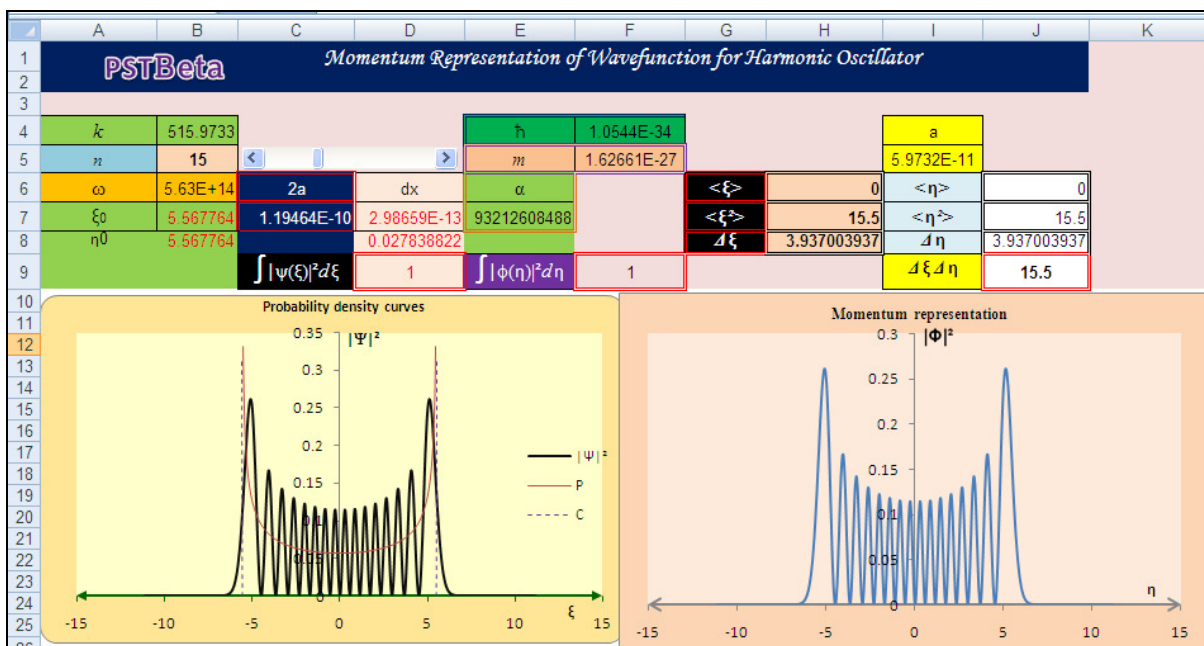The screenshot of spreadsheet used for Harmonic oscillator is shown in Fig. 1.

FIG. 1: Screenshot of spreadsheet worksheet developed for wave function and its momentum representation.

The above development of spreadsheet simulation shows that it is very easy to develop simulations using spreadsheets.

Representation of wave function in position and momentum space representation for different values of n is shown in following figures.

3. Results and Discussion

For numerical calculations of wave functions and its momentum space counterpart the limits of integration in any state were taken from three times classical limit from negative values to positive values. These values also give appreciably good accuracy because of rapidly decreasing wave functions outside the classical regions.

The distributions in position space and momentum space are shown in Fig. 2 and Fig. 3 for different values of n. In position representation classical limits are show by vertical dotted lines and classical probabilities are shown by red line curve.
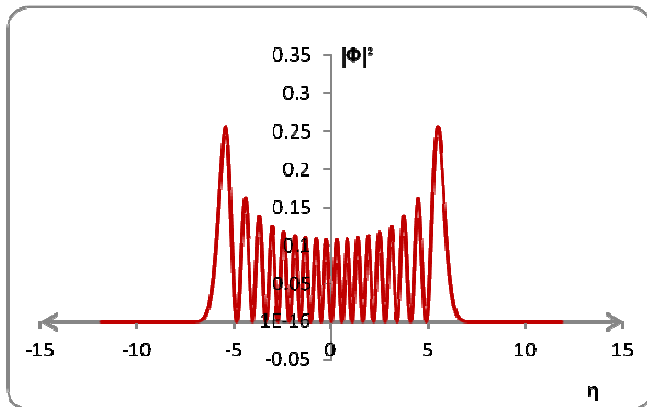

(a)Position representation
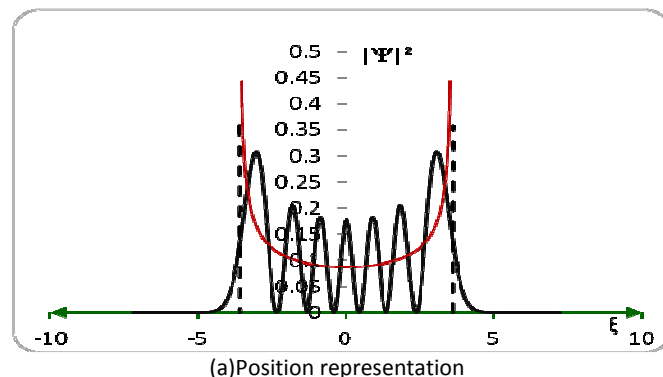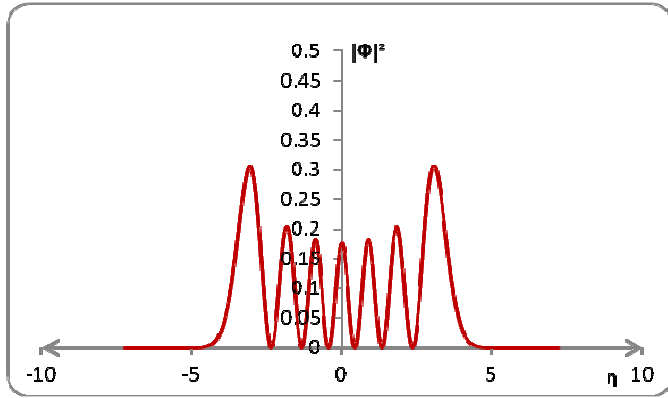
(b) momentum representation

FIG. 2: Graphical representation of probability distributions for n= 6.
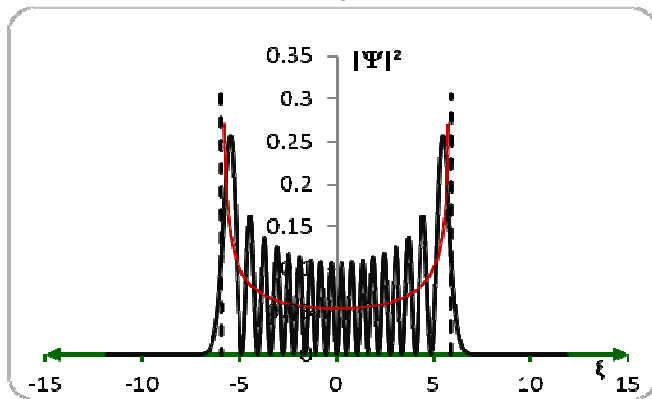
(a)   Position representation

(b)

(b)Momentum representation

FIG. 3: Graphical representation of probability distribution for n= 17.

If $|\psi(x)|^2$ is proportional to the probability density of a measurement of the particle's position yielding the value x then it stands to reason that $|\phi(p)|^2$ is proportional to the probability density of a measurement of the particle's momentum

yielding the value p. It is possible to verify Parsavel's theorem that if the function is normalized to 1 its Fourier transform also normalized to 1 [8]. Using simulation developed in this study it is found that $\sum |\psi(x)|^2\ dx = 1$ and $\sum |\Phi(p)|^2\ dp = 1$. The momentum representation has several interesting aspects. First, $|\phi(p)|^2$ is a symmetric distribution with respect to p, Consequently, the expectation value of the $<p>$ is zero, since positive and negative momenta compensate each other.

Conclusion

In the examples discussed so far, the momentum wave function is found by a numerical Fourier transform of the analytical form of the position wave function. The proposed approach makes it possible to represent eigen functions and their Fourier transforms with remarkable simplicity, and it provides valuable insight into the origin of the uncertainty principle [9].

Author expect to contribute with this approach to the development of physical insight for problems posed in the momentum representation and, furthermore, to help students to understand the different features of operators in quantum physics. The spreadsheet simulation developed in this study can easily be used to represent momentum representation of other problems in quantum mechanics. The understanding of momentum representation of wave functions is important for the students because some complex problems in quantum mechanics are easy to study in momentum representation. Such problems are scattering process, dispersion relations and the study of resonant states as solutions of a Lippmann-Schwinger equation.

References :

[1] C. Singh, M. Belloni and W. Christian, Physics Today, **59**(8), 43-49 (2006).
[2] C. Singh, (Am. J. of Phys. **69** (8), 885-895(2001).
[3] B. Cooke, Physics Educ., **32**, 80-87 (1997).

[4] J. Wagner, The Physics Teach., **45**,34-37(2007)..

[5] A.Yamani and A. Kharab. IEEE Transactions on Education, **44**(3), 292-297(2001).

[6] H. N. Nunez-Yepez, Retrived from arXiv:physics/0001030v2 on 23/8/2014.

[7] R. Liboff, *Introductory Quantum Mechanics* (Pearson Education, 2006).

[8] S. Gasiorowicz, *Quantum Mechanics* (John Wiley and Sons, 2003)

[9] F. Rioux, J. of Chem. Educ. **74**(5), 605-606 (1997).

A Century of Planck Constant Measurement

M. Goswami[1] and S. Sahoo[2]

[1]Department of Physics, Regional Institute of Education (NCERT)
Bhubaneswar – 751022, Odisha, India.
E-mail: manasigoswami1@yahoo.com

[2]Department of Physics, National Institute of Technology
Durgapur – 713209, West Bengal, India.
E-mail: sukadevsahoo@yahoo.com

Abstract

The Planck constant 'h' is a fundamental physical constant which plays an important role in understanding the behaviour of matter at the subatomic level. It is a cornerstone of the theory of quantum mechanics, which links wave-like and particle –like properties. Although the first numerical estimate of h was given by Planck himself, the American Physicist R. A. Millikan measured its value first time using the photoelectric effect in 1914. That is why the year 2014 is considered as centenary of Planck constant measurement. The measurement of the Planck constant, h, is now entering a new phase as its importance has been linked to a proposed redefinition of a kilogram unit of mass. In this article, we briefly review on measurements of Planck constant.

Keywords: Planck constant, Watt balance, Photoelectric effect, Josephson effect, Quantum Hall effect

Introduction

The Planck constant 'h' is a fundamental physical constant that plays a pivotal role in the exotic province of quantum mechanics. The constant started as a theoretical hypothesis just over 100 years ago in 1900 by Max Planck. While thinking about the conditions of equilibrium between matter and radiation, Max provided an explanation of the observed properties of black body radiation.

He assumed that atoms emit and absorb discrete quanta of radiation with energy E=hf, where f is the frequency of the radiation and 'h' is a fundamental constant of nature. Even theoretical constants have real value, so numerical measurements of 'h' within the International System of Units (SI) soon started. The SI units were originally and solely based upon artifact

standards. Precise measurement of Planck constant 'h' had created many challenges in past. In the early history of Planck constant measurements, precise voltage measurement, frequency measurement, resistance measurement etc. had added barrier to measuring 'h' in SI units [1].

The first numerical estimate of h was given by Planck himself as $h = 6.55 \times 10^{-34} \; Js$. In 1914, the American Physicist R. A. Millikan (Noble prize 1923) measured its value first time using the photoelectric effect. The result was $6.626 \times 10^{-34} \; Js$ [2]. Since last one century the numerical value of h has been determined many times using more and more sophisticated techniques. In 1969 the task group on fundamental constants called CODATA (Committee on Data for Science and Technology) was established. The 1987 report of CODATA gives the value of 'h' = $6.6260755 \, (40) \times 10^{-34} \; Js$ (which one should read as h = $(6.6260755 \pm 0.0000040) \times 10^{-34} \; Js$).

According to CODATA 2010 recommendation the accuracy of the Planck constant has now improved to disagreement with stated uncertainties in 7th digit ($6.62606957(43) \times 10^{-34} \; Js$ (which one should read as $(6.62606957 \pm 0.00000043) \times 10^{-34} \; Js$). On-going experiments measuring the value of 'h' using mass as a variable by reversing the calculation will soon overcome the last artifact barrier. The proposed revision of SI units would embed Planck constant into the definition of the Kilogram [1,3], as a fixed constant of nature. Since mass will be defined by 'h' and the speed of light 'c', obtaining a highly accurate value of the Planck constant is driving the interest in this topic. Watt balance systems are now the best method used to measure 'h'. New Watt balance 'h' and the worldwide effort to measure the Avogadro's constant [5,7] have recently become more newsworthy because of the kilogram redefinition.

A brief review of some of the early attempts to measure 'h' is indispensable because measurement of the Planck constant, h, is now entering a new phase. Transition from accepted values to newer results seems to be more interesting.

Historical Background

Planck constant was started as a hypothesis just over 100 years ago to explain the spectral distribution of 'Black body radiation' mathematically. The story begins on 19 October, 1900 when a German Physicist, Max Karl Ernst Ludwig Planck (1858-1947, Nobel 1918) presented a formula that he had guessed through his postulate that energy is quantized, to explain: why black body radiation has a finite energy spectrum. How light must have a discreteness that was not experimentally observed was a real puzzle for the scientists of those days. Although the discovery was presented to the members of the Berlin Physical Society, the lecturer himself was not able to derive the new result formally at that time. Two months later on 14 December, 1900 during a similar lecture in Berlin Planck proposed a solution to this problem. He announced revolutionary theoretical concept invented or perhaps more properly discovered by him. Planck postulated that the total energy of the cavity (the blackbody) can be attributed to the atoms of the cavity only in a very special way. He argued that each of the atoms, oscillating with frequency, can only gain a multiple of some energy E=hf, which Planck called the quantum of energy; E=hf. The letter 'h' was accepted to denote a new fundamental constant of nature. The latter date i.e. 14 December, 1900 has been considered by the physics community of the world as the birth of Planck constant – the beginning of a new era of physics, quantum physics.

Earliest Measurement (Indirect Measurement)

i)   Photoelectric effect

Besides blackbody radiation experiment there was another experiment with unexplained results; the photoelectric effect, where electrons are ejected from a metal surface under bombardment by electro-magnetic radiation. These experiments were the earliest, although indirect determination of 'h'. The unusual aspect of the effect was that the electrons had the same energy regardless of the intensity of light, but the electron energy did change with colour or frequency of light. Five year after Planck's paper, in 1905, Einstein subsequently guessed that the photoelectric effect was due to the energy being discrete or quantized [3]. He utilized Planck's mathematical relation to describe the discrete photon energy E, absorbed by or emitted from an atom as proportional to Planck constant 'h', to the frequency f as E = hf.
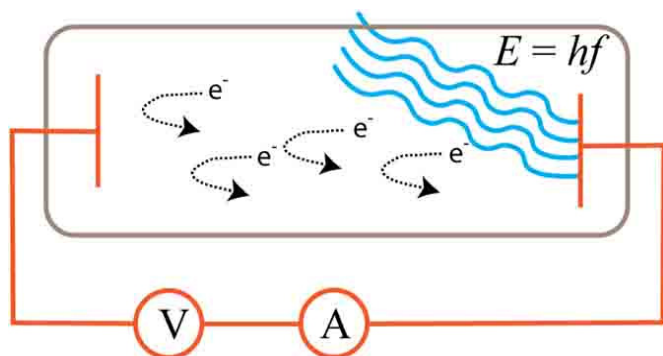

Fig.1: Photoelectric Effect.

In photoelectric effect inside a vacuum chamber, light of different frequencies ejects electrons from a metal plate. The energy of electrons is found by increasing the voltage 'V', until there is no more measured current. The energy of impinging electromagnetic energy must exceed a work function, W, a characteristics of the metal. Graphing the current stopping voltage against the impinging light's frequency produces a line where the slope is the ratio h/e, 'e' being the elementary charge. Einstein's photoelectric

equation in terms of voltage, V and work function, W describes the relation, eV = hf – W.

To determine value of 'h' a value of 'e' was needed to be measured independently. It is interesting to see here that voltage units have been historically involved in and are still intrinsic in measuring 'h'.

The value of 'h' is measured in units of energy times a unit of time i.e. in the SI system of units we have [Js], which is also known to be a unit for the quantity of action [6] and angular momentum. The first numerical [2] estimate 'h' was given by Planck himself as $h = 6.55 \times 10^{-34}$ Js.

The earliest reported photoelectric experimental results of Hughes, Richardson and Compton [1,8] in 1912, were explorations into the waves versus particle nature of the effect. Early 1913, Millikan pursued this experimental line of inquiry. In 1914, he compiled his and other's researcher's data using various physics relationships to infer the values for several constants including, e, h, Avogadro's constant N_A and Boltzmann constant k_β. The 1913 paper was the initial effort to assemble physical constant data, which constituted the Committee on Data for Science and Technology (CODATA) work of today. Millikan's 1916 paper first time published the value for $h = 6.57 \times 10^{-34}$ Js with stated uncertainty of 0.5%. This 'h' value was resulted by combining h/e measurement with his own evaluation of 'e' from the famous Oil drop experiment [3].

ii)   X-ray Diffraction Experiment

Later on several methods for measuring of h/e were improved and consequently became more significant in determining another physical constant, Avogadro's number, N_A.

In the sequence new method utilized the strong X-rays emitted from Coolidge tubes when high voltages applied to cathode tube. Duane and Hunt [1,3] used the relation $eV = hf = \dfrac{hc}{\lambda}$. The wavelength λ was measured using famous Bragg's relation $2a\sin\theta = n\lambda$ (where 'a' is grating spacing and θ is the diffraction angle). However, along with 'e', a value of 'c', the speed of light was borrowed from other experiments. From these early experiments, the relation for $\dfrac{h}{e}$ is

$$\frac{h}{e} = \lambda_{min}\,\frac{V}{c} \tag{1}$$

The method had several limitations. Particularly the voltage standard and measuring the crystal lattice spacing, a, of the diffraction material in au (atomic units) and its conversion to SI units incorporated significant uncertainties. With the data accumulated upto 1963, the inferred value [3] from the various indirect methods was

$$h = 6.62559\,(16)\times\overline{10}^{34}\ Js.$$

iii) Josephson Effect (SI units)

The discovery of Josephson effect in 1962 opened up new hope to adopt a new technique, not dependent upon the X-ray frequency and atomic lattice measurement for determination of $\dfrac{h}{e}$ ratio. By that time national volt unit was somehow standardized [8] with Weston standard Voltage cell and voltage measurement had become more précised. When a Josephson junction (junction of superconductors through a thin resistive layer) is irradiated by electromagnetic waves (microwave frequency or above) at a frequency 'f' constant voltage step, V appear across the junction as the current increases along I-V curve following the integral multiple of $\left(\dfrac{h}{2e}\right)$. The relation becomes

$$V = nf\left(\frac{h}{2e}\right), \tag{2}$$

where $\left(\dfrac{h}{2e}\right)$ ratio is the quantization of magnetic flux in superconductor. Adopting Josephson device as a voltage standard $\dfrac{h}{2e}$ ratio was evaluated in SI. The changeover from artifact voltage laboratory standard to electronic standards marked the beginning of quantum electrical metrology.

In fact the so called voltage standard controversy was a desirable prelude for international consistency in changing from kilogram mass unit artifact definition to an electronic definition based on fundamental constants. It is worth mentioning here three other important experiments that were historically linked to the determination of Planck constant. These are the (i) volt balance or electrometer (ii) the current balance/ampere balance, and (iii) Quantum Hall Effect experiment (QHE).

(i)   **SI Volt Balance**: The improved version of electrometer by Sir William Thompson and Lord Kelvin in 1868 used the electrical energy in a charged capacitor for electrostatic measurement.
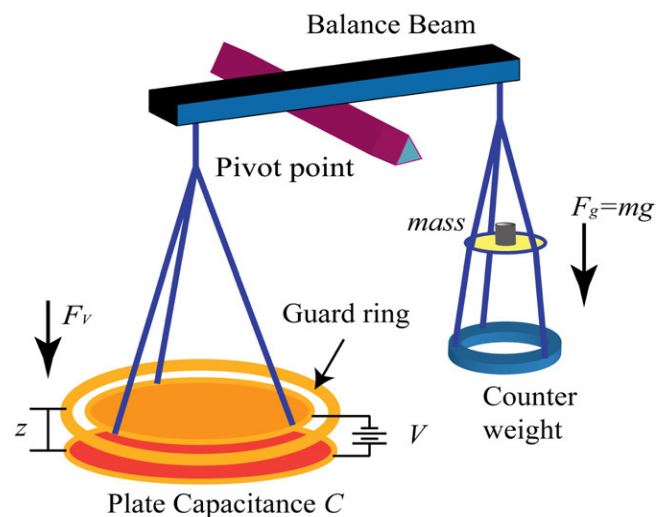

Fig.2: Absolute voltage balance diagram [1].

A gravitational force on a test mass mg is balanced by the electrical force of the differential

capacitance 'C' of two surfaces separated by a distance 'z' charged to a voltage V.

$$mg = \frac{V^2}{2}\left(\frac{dC}{dz}\right)$$

$$V = \left[2mg\left(\frac{dz}{dC}\right)\right]^{\frac{1}{2}} \quad . \tag{3}$$

The major drawbacks to this experiment were due to use of heavy electrodes to supply kilovolts of electrical potential. To avoid the limitations of the small force relative to the heavy electrodes Clothire[1] in 1965 suggested an alternative, liquid electrometer.

(ii)   SI Ampere Balance

Ampere is one of the base SI units. The definition of SI unit of current as 'Ampere' became official in 1948. The ampere is that constant current, which when maintained in two straight parallel conductors of infinite length of negligible circular cross-section and placed 1m apart in vacuum, would produce between these conductors a force equal to 2×10^{-7} Newton per meter length. The roll of ampere balance is very crucial in the history of measurement of Planck constant. It initiated the interest and motivation for independent and precise measurement of Planck's constants.

Improved Ampere balance by Rosa and Guthe [1,3] in 1912 used a pair of induction coils in a fixed position arranged vertically over one another. At the middle of these two induction coils there is a smaller movable coil. This improved geometry had the advantage of allowing the Centre coil to move to a position where the vertical force is maximum, and also varies at a minimum rate over small displacement (dz).
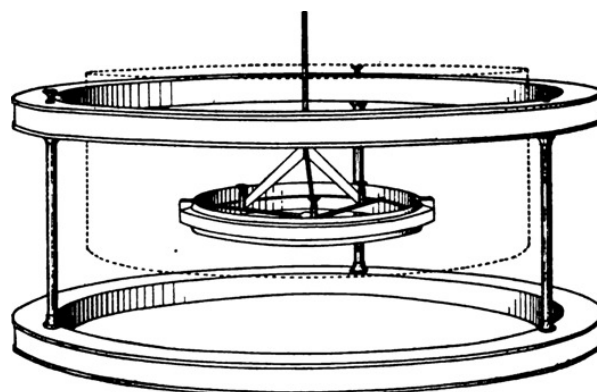

Fig.3: Absolute ampere coil configuration.

The moving coil was mechanically connected to a balance beam mass comparator. A current I_1 is passed through the fixed outer coils and current I_2, into the central movable coils. The central coil interacts with the magnetic field generated by the outer coils. This interaction creates an electromagnetic force to balance the force mg, on a reference mass 'm' due to gravity 'g'. Of course, value of g was borrowed from a separate experiment.

The basic equation is

$$mg = I_1 I_2 \frac{\Delta M_{12}}{\Delta Z} \quad , \tag{4}$$

$\Delta M_{12} \longrightarrow$ Mutual inductance between the coils at different position (ΔZ).

This established the link between the ampere and the SI units of mass, length and time. The ampere balance measured the ratio of force to current. As per suggestion of Kibble in 1976 the two quotient measurements were taken as a comparison of two different kinds of powers. Using equation-4 we can equate mechanical force multiplied with velocity (mechanical power watt) to electrical voltage multiplied with current (electrical power watt). This is the significant contribution of ampere balance which created a platform for construction of watt balance.

(iii) Quantum Hall effect Device, Resistance Standard

Interestingly while voltage and ampere controversies were coming to an end, Klaus Von Klitzing in 1980 discovered experimental evidence for quantized resistance region in Hall Effect. The equation relating the resistance steps, R in QHE device to the ratio of h/e^2 is

$$R = \frac{1}{(n)}\left(\frac{h}{e^2}\right),\tag{5}$$

where n is the quantum number for the step. For the discovery of QHE, Klaus von Klitzing received the Nobel Prize for physics in 1985.

Electrical Unit Adjustment in 1990

With the new and improved absolute volt measurement, ampere measurement, resistance measurement, the volt and resistance units were adjusted internationally in 1990 (Previous adjustment in 1969). The Josephson constant $K_J = \frac{2e}{h}$ was given a defined value of $K_{J-90} = 4835979 \times 10^9 \, HzV^{-1}$.

The symbol V_{J-90} was adopted to represent the volt as obtained via Josephson Effect, consistent with K_{J-90}. Using the new QHE system the resistance standard was adjusted and symbol Ω_{90} was adopted. Consequently a fixed value for Von Klitzing constant $R_K = \frac{h}{e^2}$ was assigned as $R_{K-90} = 25812807\Omega$ where Ω_{90} is the conventional unit.

Modern Direct Measurement of 'h'

Combining the Josephson Effect of equation (2) and Quantum Hall Effect (QHE) equation (5) Taylor in 1985 explicitly published a simple formula for h in terms of frequency.

$$\frac{V^2}{R} = \frac{\left[f\left(\frac{h}{2e}\right)\right]^2}{\left(h/e^2\right)} = f^2\left(\frac{h}{4}\right)\tag{6}$$

This equation simply relates electrical energy to Planck constant and frequency. Looking at the simplicity and direct relation to 'h', it was assumed that direct measurement of 'h' was now possible. Hence, interest in several experiments like superconducting magnetic levitation and the Joule balance was intensified for direct measurement of 'h'. However, the most popular, advance experiment for direct measurement of 'h' has been conducted using watt balance.

The Watt Balance

The watt balance scheme is a simple adaptation from the ampere balance. The concept of balance signifies here to null balancing of mechanical and electromagnetic forces, and consequently equating the computed mechanical and electromagnetic power. The four criteria which are basically required for the watt balance is summarized in the recent paper [1]

    a.   A Stable magnetic field needs to be generated where the spatial gradient of flux density $\left(\vec{\nabla}\phi\right)$ has a preferential geometry.

    b.   Considering the opted stable magnetic field an induction coil operating at reference values for voltage, current, resistance and mass is designed.

    c.   The coil needs to be connected to a support mechanism that has balancing pivot point, so the coil moves with small driving force.

    d.   The whole mechanism is to be aligned in such a way that the coil
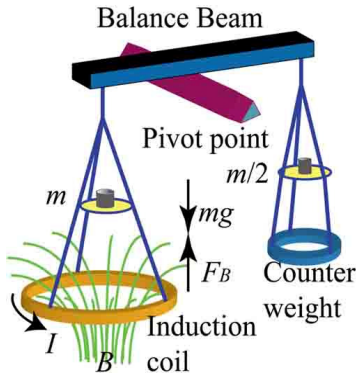
moves nearly vertical over a long distance.

Fig.4: The watt balance scheme

To start with, without test masses the main coil with no current passing through it is first balanced with a counter weight. Then in the force mode (with current in main coil) a tare mass on the counter mass side, of half the test mass is initially balanced by the downward component of the electromagnetic force. This is because the electromagnetic applied force is half the total gravitational force on the test mass. The balance beam facilitates the coil to move mostly vertical. After this the current is reversed to balance the main test mass. Current reversal not only eliminates voltage and balance force off sets, but also maintains constant Ohmic heating of the coil during weighing mode.

Basic Watt Equation

The differential Lorentz force equation describes a gravitational force on mass 'm' as equal to a force on a coil with a current I, within a magnetic flux density dependent on the z-gradient

$$F_z = mg = -I\frac{\partial \phi}{\partial z} \qquad (7)$$

In the differential form of Faraday's law a coil produces a voltage V (in fact emf ϵ), when moving at a velocity $\frac{\partial z}{\partial t} = v_z$.

$$V = -\frac{\partial \phi}{\partial t} = -\frac{\partial \phi}{\partial z}\frac{\partial z}{\partial t} = -v_z\frac{\partial \phi}{\partial z} \qquad (8)$$

Assuming magnetic flux gradient to be identical in equation (7) and (8) we can have the two equations

$$mgv_z = VI = \frac{V^2}{R} \qquad (9)$$

where I is measured as the voltage drops (V), across a reference resistance R.

Expanding equation (6) (ignoring quantum numbers)

$$\frac{V^2}{R} = \frac{(f\,{}^h\!/_{2e})^2}{({}^h\!/_{e^2})} = f^2\frac{h}{4}[W] \qquad (10)$$

Using $\left(\frac{2e}{h}\right)^2 = K_{J-90}^2$ and $\frac{h}{e^2} = R_{K-90}$, we can rewrite equation (10) as

$$\frac{V^2}{R} = \frac{f^2}{K_{J-90}^2 R_{K-90}}[W_{90}] \qquad (11)$$

Comparing (10) and (11)

$$[W_{90}] = \frac{h}{4}\left(R_{K-90}\,K_{J-90}^2\right)[W]. \qquad (12)$$

Thus putting conventional electrical measurements into the SI units of mechanical power measurements requires a conversion from [W$_{90}$] to [W], given by equation (12).

From equation (9), we have

$$mgv_z = \frac{V^2}{R} = \left(\frac{V^2}{R}\right)_{90}[W]_{90}$$

$$\left[\frac{mgv_z}{\left(V^2/R\right)_{90}}\right] = [W_{90}] \qquad (13)$$

$$\frac{mgv_z}{\left(V^2/R\right)_{90}} = \frac{h}{4}\left[R_{K-90}K^2_{J-90}\right]$$

using equation (12)

$$h = \frac{mgv_z}{\left(V^2/R\right)_{90}}\frac{4}{\left(R_{K-90}K^2_{J-90}\right)} \qquad (14)$$

It is important to note from equation (14) that, measurement of 'h' does not depend upon any adopted values for K_{j-90} and R_{k-90}. Recently [8], a watt balance at the National Institute of Standards and Technology (NIST) has determined the value of Planck constant as $h = 6.62606979(30) \times 10^{-34}$ Js.

Conclusion

The Planck constant plays an important role in understanding the behaviour of matter at the subatomic level. It is a cornerstone of the theory of quantum mechanics, which describes the strange behaviour of particles at this level. The accuracy of Planck constant has recently become a newsworthy issue because of proposed revision of SI units. Since indirect method (1914) to direct method (2010) the Planck constant has been measured with ever better resolution (Fig.5).
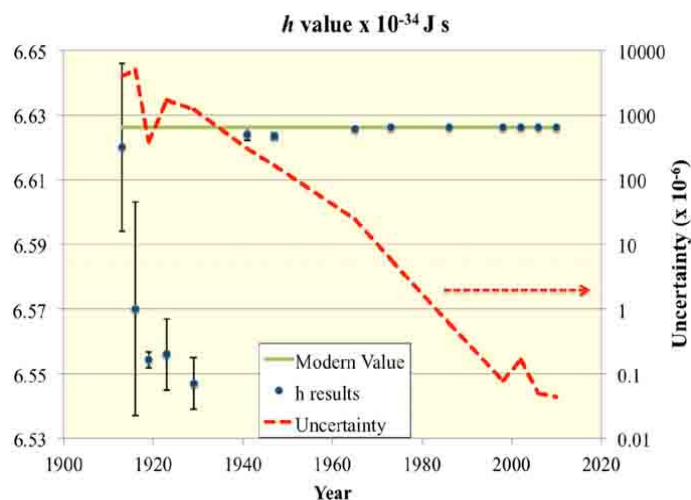

Fig.5: A graph summarizing the complete history of Planck constant determinations [1]. Dotted line shows the decrease of uncertainty over the years.

Several of the base units within the SI system are in the process of being redefined with an aim of linking the units to fundamental constants of nature [4,6]. This is the proposal of Bureau International des Poids et Mesures (BIPM-2010). The proposed revision of SI units would embed Planck constant into the definition of kilogram as a fixed constant of nature. In this present article, brief review on measurements of Planck constant has illuminated its impressive history. It is also amazing to realize that the best measurement of Planck constant 'h', which is purely a quantum concept, is attainable by a watt balance which combines an 'Old Classical Physics' involving force balance, electromagnetic induction/ interaction etc. to a new quantum based time, frequency and electrical measurements. Many review articles are available in the literature but original papers are hard to find. However, the conclusion is that as measurement uncertainties pertaining to Planck constant has declined substantially (few parts in 10^8) from watt balance experiments and Avogadro determination, its importance has been linked to a proposed redefinition of a kilogram unit of mass.

References

1. Steiner Richard, History and progress on accurate measurements of the Planck constant, *Rep. Prog. Phys.* 76 (2013) 016101.
2. J., Makowski Adam, A century of the Planck constant, *Phys. Educ.* 35(1) (2000) pp. 44–53.
3. Singh, A. et al, Certain investigation regarding variable physical constants, *Int. J. Res. Rev. Appl. Sci.* 6 (2011) pp. 18–29.
4. Calogero, F., Cosmic origin of quantization, *Phys. Lett. A.* 228 (1997) pp. 335-346.
5. Andreas, B, Determination of the Avogadro constant by counting the atoms in a ^{28}Si Crystal, *Phys. Rev. Lett.* 106 (2011) 030801.

6. Quincey Paul, Planck constant as a natural unit of measurement, *Phys. Educ.* 48(5) (2013) pp.597-600.

7. Becker, P., History and progress in the accurate determination of the Avogadro constant. *Rep. Prog. Phys.* 64 (2001) 1945.

8. Schlamminger, S. et al., Determination of the Planck constant using a watt balance with a superconducting magnet system at the National Institute of Standard and Technology, *Metrologia* 51 (2014) S15 [arXiv:1401.8160 [physics.class-ph]].

*****

Elementary remarks on the ambiguous explanation of pressure in chemical thermodynamics

Yukio Kobayashi

Department of Information Systems Science
Faculty of Engineering
Soka University
Tokyo 192-8577, Japan.
koba@t.soka.ac.jp

Abstract

At the collegiate level of chemical thermodynamics, action-reaction pairs are not explicitly described, which results in an ambiguous explanation of the procedures to vary the volume of a system. Pedagogically, it is essential to specify not only the magnitude of forces, but also the object that applies the force and the object that experiences the force. The physical meanings of some of the equations in thermodynamics should be explained in terms of elementary mechanics. From these viewpoints, it is indispensable to combine physics education and chemical education at an elementary level of science teaching.

1 Introduction

In standard physical chemistry textbooks for undergraduate students [1, 2, 3], some papers on physics education [4], and some papers on chemical education [5], the work performed in varying the volume of a system is explained at an elementary stage, but the descriptions are unexpectedly ambiguous. From a pedagogical standpoint, the physical meanings of some quantities in chemical thermodynamics should be explained on the basis of elementary mechanics. Many textbooks, however, give confusing descriptions of the work done on the system, because the action-reaction

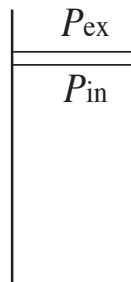pairs are not explicitly described, as seen from Figure 1.

Figure 1: The pressure of a gas inside the cylinder is P_{in} and the external pressure is P_{ex}.

To examine this circumstance, the following elementary problem is given from the standpoint of mechanics.

> Consider the gas inside of a cylinder with a piston area S (Figure 2). The internal pressure exerted on the piston by the gas is P and the external pressure exerted on the piston by the surroundings (e.g., the atmosphere and/or an external agent such as the hands of a person) is P_{ex}. The volume swept during an infinitesimal expansion is denoted as dV, where $dV = Sdx$ and dx is the displacement of the piston. Does PdV, $-PdV$, or $-P_{ex}dV$ represent the work done on the system (i.e., the gas in the cylinder)?

Figure 2: Internal pressure and external pressure. PS is the force exerted on the piston by the gas. $-PS$ is the force exerted on the gas by the piston. $-P_{ex}S$ is the force exerted on the
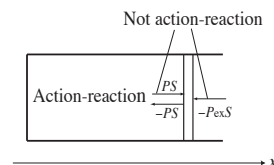
piston by the surroundings. PS and $-PS$ constitute an action-reaction pair. PS and $-P_{ex}S$ act on the piston in a state of equilibrium.

This problem is difficult to solve for some students, because PdV, $-PdV$, and $-P_{ex}dV$ are frequently confused with one another due to the ambiguous descriptions in the above-cited physical chemistry textbooks and papers. These quantities should be distinguished according to elementary mechanics. The system does not experience pressure directly from the surroundings, but rather via the piston [6]. If we consider the work done on the system to be $-P_{ex}dV$ following the above textbooks, the equation for the equilibrium of the piston, $PS + (-P_{ex}S) = 0$, is essentially meaningless, as shown in the Section 4.

2 Representation of the Work Done on the System

The object that performs the work should be described to avoid confusion with the three quantities PdV, $-PdV$, and $-P_{ex}dV$. It is important to distinguish the following quantities: the work done on the system by the piston ($-PdV$), the work done on the piston by the system (PdV), and the work done on the piston (not on the system) by the surroundings ($-P_{ex}dV$) as shown in Figure 2. During a quasistatic process, these

quantities are equal in magnitude. For this reason, some textbooks state that the work done on a system is $-P_{ex}dV$ [1], but according to elementary mechanics [10], this description is not necessarily accurate. Irrespective of whether the piston is in equilibrium or not, $-P_{ex}dV$ and $-PdV$ are conceptually different quantities.

The following description is ambiguous from the standpoint of elementary mechanics.

> The force exerted on the piston by the surroundings is $-P_{ex}S$. When the system expands through a distance dx, the system moves the piston against the force $-P_{ex}S$. The work done on the surroundings by the system is $P_{ex}dV$.

The phrase 'on the surroundings by the system' seems to indicate that the system exerts the force directly on the surroundings. From a pedagogical standpoint, this explanation contains a jump in logic, which can be described as follows. Although the forces PS and $-P_{ex}S$ act in opposite directions and have the same line of action, they do not constitute an action-reaction pair. Both forces act on the same body (the piston), whereas an action and its reaction act on separate bodies according to Newton's third law of motion. When a piston is in equilibrium, the forces PS and $-P_{ex}S$ are equal in magnitude. Even when a piston is not in equilibrium, the force exerted on the system by the piston and the force exerted on the piston by the system are equal in magnitude. The system exerts a force PS on the piston and the piston exerts a force $P_{ex}S$ on the surroundings. The forces $P_{ex}S$ and $-P_{ex}S$ constitute an action-reaction pair, because $P_{ex}S$ is the force exerted on the surroundings by the piston and $-P_{ex}S$ is the force exerted on the piston by the surroundings.

It is important to distinguish the forces shown in Figure 2, although $-PdV$ and $-P_{ex}dV$ are equal in magnitude.

Table 1   Forces on what by what

Force	On	By
PS	piston	system
$-P_{ex}S$	piston	surroundings
$P_{ex}S$	surroundings	piston

The following is another example from physics education. A weigh scale indicates not the gravitational force exerted on a body, but the force exerted on the weigh scale by the body, although these two forces are in equilibrium (they have equal magnitudes). If these two forces are not separately identified, it will be impossible to understand the meaning of the value from the weigh scale during accelerated motion. This value is different from that of a weigh scale at rest. The value is determined by the force exerted on the weigh scale by the body. This force is not equal in magnitude to the gravitational force during accelerated motion. Physics educationists should specify not only the magnitude of a force, but also the object that applies the force and the object that experiences the force.

3   Remarks on the First Law of Thermodynamics

The interpretation of the physical or chemical significance of an equation depends on the form that is used to express it. For example, the equation for the equilibrium of a body in statics, $m\boldsymbol{a} - \boldsymbol{F} = \boldsymbol{0}$, has a different physical significance

from the equation of motion based on Newton's second law of motion in dynamics, $m\boldsymbol{a} = \boldsymbol{F}$, despite these equations being algebraically equivalent [7, 8]. The term $m\boldsymbol{a}$ in the equation of equilibrium is recognized as an inertial force, whereas the equation of motion indicates that the acceleration determined by the mass of the body results from the sum of the exerted forces, $\boldsymbol{F}$. Unfortunately, some educationists are not necessarily convinced that $m\boldsymbol{a} - \boldsymbol{F} = \boldsymbol{0}$ has a physical significance that is different from that of $m\boldsymbol{a} = \boldsymbol{F}$.

Analogously, the meaning of the first law of thermodynamics depends on how it is expressed algebraically. The change in the total energy of a system du is equal to the sum of the energy added to the system in the form of absorbed heat $d'q$ and the work done on the system $d'w$:

$$du = d'q + d'w. \tag{1}$$

In Eq. (1), $d'w = -PdV$ (see the previous section), although some textbooks give $d'w = -P_{\mathrm{ex}}dV$ [1, 2]. In contrast, the heat absorbed by a system $d'q$ yields the energy change of the system du and the work done on the piston by the system $-d'w$:

$$d'q = du + (-d'w), \tag{2}$$

in which $-d'w = PdV$.

As $-d'w$ in Eq. (2) is represented by a force exerted on the piston by the system PS, $d'w$ in Eq. (1) transformed by Eq. (2) can be determined by the force exerted on the system by the piston $-PS$. However, some textbooks describe $d'w$ in Eq. (1) as the force exerted on the piston by the surroundings $-P_{\mathrm{ex}}S$, because P and P_{ex} are equal in magnitude. Consequently, students will be confused if they fail to understand that PS and $-P_{\mathrm{ex}}S$ constitute an action-reaction pair of forces, if the piston is ignored, during a quasistatic process (see the end of the next section).

4 Physical Meaning of the Internal Pressure

The equation of state for an ideal gas is taught in the form $PV = nRT$, where n is the amount of gas at temperature T, P is the internal pressure exerted on a piston by the system with a volume V, and R is the gas constant. The meaning of the internal pressure becomes clear when the equation is transformed from $PV = nRT$ to $P = (n/V)RT$. The internal pressure depends on the number density and the temperature of the system. The internal pressure does not need to be generated by a piston in the following, but it is easier to consider that the pressure is generated via a piston. The internal pressure is largely determined by the average number of strokes performed by the piston. The number density and the temperature of the system can be adjusted to maintain a constant internal pressure, as expressed by $dP = d(n/V)RT + (n/V)RdT$.

The external pressure is the sum of the pressure exerted on the piston by the atmosphere and the pressure due to an external agent, such as the hands of a person. The external pressure is independent of the number density and the temperature of the system, although the external pressure has the same magnitude as the internal pressure when a piston is in equilibrium. Measuring $-P_{\mathrm{ex}}$ is the only way to determine the magnitude of P (or $-P$). We can obtain the work done on the system as $d'w = -PdV$ by using Newton's third law of motion; this expression is independent of $P_{\mathrm{ex}}S$. This equation can be applied to a piston in equilibrium, $PS + (-P_{\mathrm{ex}}S) = 0$, to determine P in $d'w = -PdV$. If P and P_{ex} are not distinguished, the equation for the equilibrium of the piston cannot be written. During a quasistatic process, the piston enables us to mea-

sure P through P_{ex} and to calculate the work done on the piston by the surroundings from the displacement of the piston by expressing $d'w$ as $-P_{\text{ex}}dV$.

There is another view in standard textbooks on chemical thermodynamics as follows. When a piston is in equilibrium, we can also consider that the piston transmits a force from the surroundings to the system and vice versa. The role of the piston is frequently interpreted as follows: PS exerted on the piston by the system (the gas) equals $-P_{\text{ex}}S$ exerted on the piston by the surroundings in magnitude, because the piston is in equilibrium. As $-PS$ exerted on the system (the gas) by the piston is always equal in magnitude to PS according to Newton's third law of motion, in this special case of equilibrium, $-PS$ also equals $-P_{\text{ex}}S$; that is, the force exerted on the system by the piston is equal to the force exerted on the piston by the surroundings. The piston is thus considered to transmit the total force exerted on the piston by the surroundings to the system. If we adopt this point of view, it is not necessary to consider the piston itself; thus, we can also consider that the surroundings exert a force $-P_{\text{ex}}S$ directly on the system. The reaction to this force is the force exerted by the system on the surroundings when the piston is not taken into consideration. We can also write $-P_{\text{ex}}S$ for the inner surface of the system (the gas) while not taking the piston into consideration. However, it is inconsistent to refer to the piston only for the measurement of the internal pressure exerted on the piston by the gas, P, to calculate $-PdV$, when only the gas and the surroundings are taken into consideration instead of the system (the gas), the piston, and the surroundings.

The same approach is also applied to the following mechanics problem in some textbooks on elementary physics [10]. Two blocks are connected by a light inextensible string and are placed on a smooth horizontal table. The force exerted on the first block due to the string running to the second block constitutes an action-reaction pair with the force exerted on the second block due to the string running to the first block. This interpretation is false. If the mass of the string is not negligible compared to the mass of the blocks, these two forces will not be equal in magnitude and thus they do not constitute an action-reaction pair. Newton's third law of motion is independent of the mass of the string [11]. Even if the string is light, the former force is applied to the first block by the string, whereas the latter force is applied to the second block by the string.

Pedagogically, it is essential to always interpret the physical meaning of the internal pressure by following elementary mechanics. A comparison between the dynamical system of a massless spring connected to a particle and the thermodynamic system helps students understand the internal energy of the system, as well as the action-reaction pair of forces. A particle and the spring correspond to the piston and the gas, respectively.
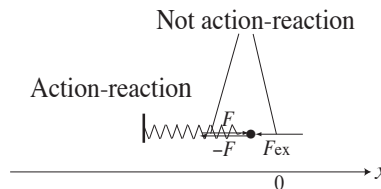

Figure 3: A massless spring connected to a particle. In this figure, the spring is compressed. Compare this figure to Figure 2.

It is important to distinguish the following three forces: F, the force exerted on the par-

ticle by the spring; $-F$, the force exerted on the spring by the particle; and F_{ex}, the force exerted on the particle by an external agent such as the hands of a person. The internal energy of the gas is comparable to the energy stored in the spring. During a quasistatic process to compress the spring, the work done on the particle by the agent is cancelled exactly by the work on the particle by the spring, and thus the energy is not stored in the particle. The spring, however, stores the energy by the work on the spring by the particle. Similarly, the piston transmits the energy from the surroundings to the gas and thus the same amount of energy is stored in the gas.

5 Concluding Remarks

According to some textbooks on elementary chemical thermodynamics, the forces PS and $-P_{ex}S$ constitute an action-reaction pair by regarding the piston, the atmosphere, and the hands of a person as the surroundings. In this approach, $-P_{ex}S$ is exerted on the system by the surroundings. However, it is difficult to consider that the magnitude of $P_{ex}S$ is equal to the magnitude of the force exerted on a piston by the atmosphere and the hands of a person. The work done on the piston by its surroundings differs physically from the work done on the system by the piston. These textbooks employ ambiguous reasoning to derive the work done on a system, because they do not explicitly introduce the concept of an action-reaction pair. Following the standard textbook [12], we must specify the *force on what by what* and the *work on what by what* when the force and work are discussed.

Through the problem discussed in this article, it is pedagogically essential to combine physics education and chemical education at an elementary level when teaching science. The basic notion of an action-reaction in elementary mechanics at the high school level is not fully reflected in chemical education. Reconsidering the chemical thermodynamics from a physics standpoint helps educationists and students understand the basic mechanism of the dynamical process.

References

[1] P. W. Atkins. Physical Chemistry (Freeman, 1994)

[2] D. Eisenberg and D. Crothers. Physical Chemistry with Application to Life Science (Benjamin, 1979)

[3] E. B. Smith. Basic Chemical Thermodynamics (Oxford Science Publications, 1990)

[4] A. Kinoshita (2007). J. J. Appl. Phys. Educ. 31, 25-29

[5] G. L. Bertand (2005). J. Chem. Educ. 82, 874-877

[6] I. Sakama, T. Tani, and Y. Yamamoto. Daigaku Nyushi Hissyu Butsuri (Sundaibunko, 1980) [in Japanese]

[7] Y. Kobayashi (2008). Eur. J. Phys. 29, 599-606

[8] Y. Kobayashi (2012). Phys. Educ. 28, 6

[9] R. Sears and W. Zemansky. Modern University Physics (Addison-Wesley, 1960)

[10] F. W. Constant. Fundamental Laws of Physics (Addison-Wesley, 1963)

[11] K. Tomiyama. Butsurigaku heno Michi (Iwanami, 1974) [in Japanese]

[12] C. Kittel, W. D. Knight, and M. A. Ru-

derman. Berkeley Physics Course Vol. 1, Mechanics (McGraw-Hill, 1973)

Spatial Characterization of LED's Irradiance using Ordinary Detectors

A. Raghu[1], T. Shivalingaswamy[1], P. E. Rashmi[2]

[1]Post Graduate Department of Physics, Government College (Autonomous), Mandya 571401, India.
[2]Department of Physics, Government College for Women, Mandya 571401, India.
raghua4@gmail.com
(Submitted: 16-07-2014)

Abstract

In this article, irradiance profiles of common LEDs along the beam propagation direction and in a plane perpendicular to propagation direction are studied using inexpensive photo detectors, viz., photo diode and photo transistor. Different methods used in Indian institutes for the analysis of radiation are discussed along with their limitations and advantages. General considerations required to characterize anisotropic radiators using ordinary detectors are discussed. It is found that, out of the two detectors photo transistor works better for LEDs radiations. These results are compared with results obtained from another anisotropic radiator, viz., open laser diode and one isotropic radiator incandescent lamp.

1 Introduction

Irradiance from a point source varies in a predictable way as a function of distance and angle. i.e., such radiation is isotropic and their irradiance describe inverse square law in all directions [1]. Actual nature of irradiance from any given source can be determined with the help of a well calibrated detector [2]. On the other hand, a source that describes standard radiation behaviour can be used to test the performance of a given detector. Often, low cost detectors and radiation sources that are available in the market fail to satisfy

standardization tests. If a system of an uncalibrated detector and an uncalibrated source is provided, then its working status needs to be tested before using it for any further studies. This article attempts to address precisely this difficulty faced by the people who use such systems. Working of such a system is examined by the study of source' irradiance from a given detector as a function of separation distance between them by three methods. In addtion, this paper attempts to compare these methods and attempts to rectify the limitations of such measuring systems.

Most commonly available LEDs are used here and they are normally anisotropic radiators. While a small part of radiation is emitted by an LED in a hemispherical shape, a large amount of its radiation is emitted in a direction perpendicular to the emitting surface. However, even such radiation beam from LED is not unidirectional, instead it diverges from the exit end of LED. Encapsulation of LED provides certain radiation pattern by acting as a lens and it also provides mechanical protection to LED [2]. The typical Lambertian radiation pattern from an ordinary encapsulated LED shows that light energy is generally emitted in an angular range between 4° to 160° from the direction of maximum light for various encapsulations [2, 3, 4]. Not limitting to this angular range, there are special LEDs with wide angle of emission extending up to nearly 360° [5]. In order to understand the irradiance nature from a particular LED, it is necessary to have the knowledge of irradiance profile of that LED in all spatial directions [2].

Irradiance of LED along its propagation direction is expected to describe some power law with distance. A few reports of optical power law measurements using LEDs as radiation sources are available. Rajesh *et al* have used common LED as source and a photo diode as detector, but they have only plotted $(1/i_o)^{1/2}$ versus d, without reporting the exponent of distance with radiation [6]. Kutzner *et al* used common LED as source and another LED as a photo detector and obtained an average exponent of -2.23 [7]. Wanser *et al* have used light (intensity) to frequency converters as detectors and two different types of special LEDs for their study and obtained an exponent of ≈ -2.00 with high accuracy data [5]. Note here that, these two are special LEDs designed for special applications and they are different from the LEDs which are characterized by nearly unidirectional emission pattern. The latter type of LEDs are used in this work. In addition, inexpensive and uncalibrated photodiode and phototransistor are used here as detectors so that this experiment can be implemented with a modest budget in any undergraduate institutions.

2   Theory

A light detector always measures irradiance of source and its output current i_o is linearly proportional to the amount of irradiance E sensed by it [8].

$$\text{i.e., } i_o \propto E \qquad (1)$$

The irradiance E is a measure of the concentration of the optical power. It is defined

as radiant flux (power) received by the unit area of the irradiated surface of the detector [1]. Radiant intensity I is the radiant flux emitted per unit solid angle. Given a point light source, for normal incidence, the irradiance E, Radiant intensity I and separation distance d are related through the relation [1, 9].

$$E = I/d^2 \qquad (2)$$

A plot of E versus $1/d^2$ should give a straight line with I as its slope. The objective of this method is to observe, how best the data fit into a straight line. A reasonably good conformity to the plotted data corroborates inverse square law.

Equation (2) is true for radiations from an isotropic radiator like a point source. At this point, a question arises; does radiation from an anisotropic radiator like LED follow (2) or not? If not, how its irradiance is related with d? These are addressed below.

Let 'n' be the exponent of distance between detector and source, such that,

$$E \propto 1/d^n \implies E = k'/d^n \qquad (3)$$

Where 'k'' is the proportionality constant. Taking log on both sides of (3),

$$\log E = \log k' - n \log d \qquad (4)$$

It is clear from (4) that, a plot of $\log E$ versus $\log d$ should yield a straight line with the true power index 'n', as its slope.

In this article, i_o is used instead of E, according to (1). If there is any factor between i_o and E, then it is expected to merge with
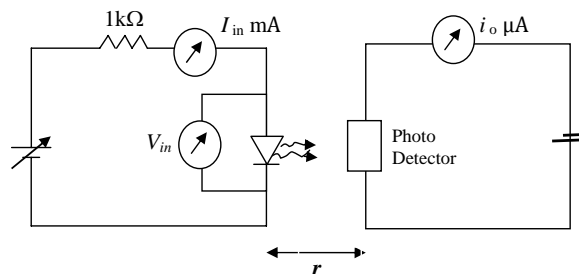

Figure 1: Circuit connections for the investigation of LEDs radiation.

the proportionality constant k' through the relations, (1) and (3) to a new constant k. Then k is directly related to radiant intensity I and the relation (4) modifies to,

$$\log i_o = \log k - n \log d \qquad (5)$$

It is clear from (5) that using i_o instead of E, does not affect the estimation of n in any manner. More rigorous approach to know the true power law of radiation was developed from a two aperture approximation model for LEDs radiation and a modified inverse square law was used to obtain more consistent results [2, 10].

3 Description of the Setup

The circuit connections are made as shown in figure 1. Mounted LED and detectors are placed on a graduated optical rail, which helps in their alignment and also in smooth variation of the distance between them. A photo detector mounted on a XYZ translation stage with micrometers of LC 10 μm

(=0.01 mm) is used to scan the LED's radiation beam. Here blue and red LEDs are used for characterization. To study the LED's radiation pattern in three dimensions, two different types of detectors are used, viz., a reverse biased (-5 V) silicon photo diode (part # PD-M-LK2-SHARP BS520) and a collector emitter reverse biased (-5 V) silicon based photo transistor (part # PT-M-LK-EVERLIGHT PT 333-3C) [11]. Photo transistor is enclosed in a pinhole chamber to avoid the effect of ambient radiation on the measurement. While using photo diode proper care has been taken to reduce the effect of ambient light on the measurements. The size $2R'$ (R'-radius) of the pin hole aperture in front of the photo transistor is ≈ 0.7 mm and therefore the exposed area A of the photo transistor is $\pi(R')^2 = 0.385$ mm^2 [11]. Active area A of the photo diode is 5.32 mm^2 [11]. LEDs, photo detectors and all opto-mechanical equipment are from Holmarc, India.

In addition to anisotropic LED sources, another anisotropic radiator viz., a laser diode without collimating lens (Holmarc, 3 mW, 650 nm) and an isotropic radiator, 100 W incandescent bulb are used in the study. A typical laser diode output beam is highly diverging with a large divergence angle ($\theta_\perp$, full width at 50 % intensity) in the direction perpendicular to the rectangular junction of diode, and it diverges with a small angle ($\theta_\parallel$) in the parallel direction [12]. For the diode laser used in this study $\theta_\perp = 38°$ and $\theta_\parallel = 10°$ [11].
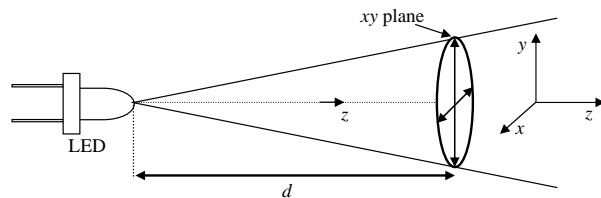

Figure 2: Schematics displaying x and y scanning method of a diverging radiation pattern from LED in a plane at a distance d and its irradiance is studied along z as a function of separation distance d.

4 Experimental Procedure

An irradiance pattern describes the relative light strength in a given direction from its source. In order to study irradiance pattern of an LED, it is driven with a sufficiently high power to obtain an intense light output. At a fixed distance, the projection of LED's radiation beam on a plane is nearly a circle or an ellipse of low eccentricity. If z is taken as the direction of the propagation of LED's radiation, then the radiation pattern of LED in three dimensions can be characterized first by scanning the beam in two mutually perpendicular directions x and y, in the xy plane (figure 2) at a fixed d. This is referred as the first characterization. The variation of LED's irradiance along z direction as a function of d is referred as second characterization.

In the first characterization, two detectors are placed one after the other at a distance of $d = 3$ cm from LED in a plane perpendicular to the propagation of beam. In this plane, radiation pattern is scanned using a
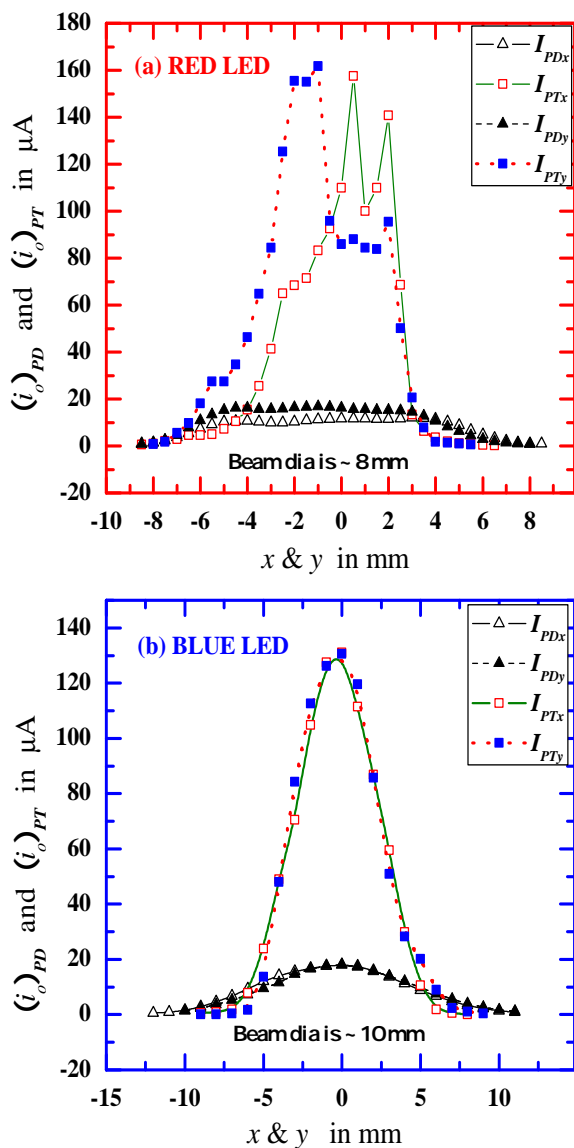
Figure 3: Radiation pattern of LEDs as measured with a photo diode (PD, △ and ▲) and with a photo transistor (PT, □ and ■) in two mutually perpendicular directions x and y, shown as a plot of current (in μA) as a function of x and y for (a) red LED and for (b) blue LED.

XYZ translation stage in steps of 1 mm along x and then along y, till detector senses the radiation. Care is taken to ensure that both the detectors pass through an approximate center of the pattern in both the scans.

Since LED emits radiation anisotropically, one must choose a reference point on irradiance for its study along beam propagation direction 'z'. Peak irradiance of its pattern is chosen for two reasons:

1. light can be detected even at longer distances and

2. alignment of peak irradiance (optical symmetry axis) from a diverging beam in a given direction is simpler than at any lower irradiance level.

Whenever radiation from LED has a single peak, LED is aligned in such a manner that its peak irradiance is along the center of optical rail. Otherwise, misalignment of radiation from an anisotropic radiator like LED leads to faulty results. Separation distance is increased in suitable steps from 5 cm to around 45 cm and corresponding output current data is collected. Analysis of this data is discussed under the results section.

However, use of this procedure for a study of radiation pattern with multiple peaks is cumbersome. Normally in such patterns, peaks are off the beam center which lead to problem of aligning the diverging LED's radiation beam. When a peak of such radiation is aligned, error in the measured data increases.

5 Results and Discussions

5.1 Irradiance profile of LED

5.1.1 In a plane perpendicular to beam propagation:

The irradiance patterns of red and blue LEDs with photo diode and photo transistor are measured in two directions x and y, at a distance of $d = 3$ cm and they are shown in figure 3. The radiation pattern of blue LED has a single peak which is symmetric with respect to peak (figure 3(b)), whereas red LED has two peaks in each measured directions x and y and their positions are not the same (figure 3(a)). For a given irradiance, the current data from a photo transistor has a gain factor 'G' with respect to a photo diode [8, 13]. Due to this, for a given irradiance, signal from a photo transistor is stronger than that from a photo diode in all the measurements.

The beam diameter (spot size) can be estimated from 3(b) as that width which contains almost 85% of the total light power [9]. The width of the beam along x is nearly the same as that along y, suggesting a circular pattern for blue LED with a diameter of nearly 10 mm at $d = 3$ cm. In the case of red LED this estimation is slightly difficult due to multiple peaks in its irradiance pattern, which are attributed to defect in the manufacturing process of LED. Its diameter is found to be ≈ 8 mm at $d = 3$ cm.

Normally, irradiance profile is represented in polar plots which do not depend on d

[2, 3]. Plane angle θ is estimated from the peak intensity as $\theta_x = \tan^{-1}(x/d)$ or $\theta_y = \tan^{-1}(y/d)$. Angular distributions of LED's radiation pattern is represented by $\theta_{1/2}$ values which are the view angle when radiant intensity is half of the value at $\theta = 0°$. More consistent $\theta_{1/2}$ values of LED's radiation are obtained at separation distances greater than 10 cm [2]. The $\theta_{1/2}$ values are slightly inconsistent and hence slightly higher at lower separation distances [2]. Measured '$\theta_{1/2}$' value with this method for blue LED is 14° at $d = 3$ cm. Therefore it is expected that the consistent $\theta_{1/2}$ for the blue LED to be slightly lower than 14°. For an LED with $\theta_{1/2} > 10°$ the angular dependence of irradiance on power law measurements can be neglected [2]. Therefore, such measurements are not carried out here for the LEDs studied for which $\theta_{1/2} > 10°$.

5.1.2 Along beam propagation:

Along beam propagation direction z, radiation is expected to describe some power law. Therefore, initially, three detectors viz., two photo diodes (PD1 and PD2) and a photo transistor (PT) are used for this purpose.
Direct Method:
A plot of i_o versus $1/d^2$ is drawn for all the three detectors for red LED and two detectors (PD1 and PT) for blue LED which are shown in figure 4(a) and figure 4(b) respectively.

A linear fit to data is carried out for all the data sets using Origin software (Version 8.1, OriginLab Corporation). Apparently the data describe straight lines as shown in figure 4(a), but the slopes 'k' of the data sets are not
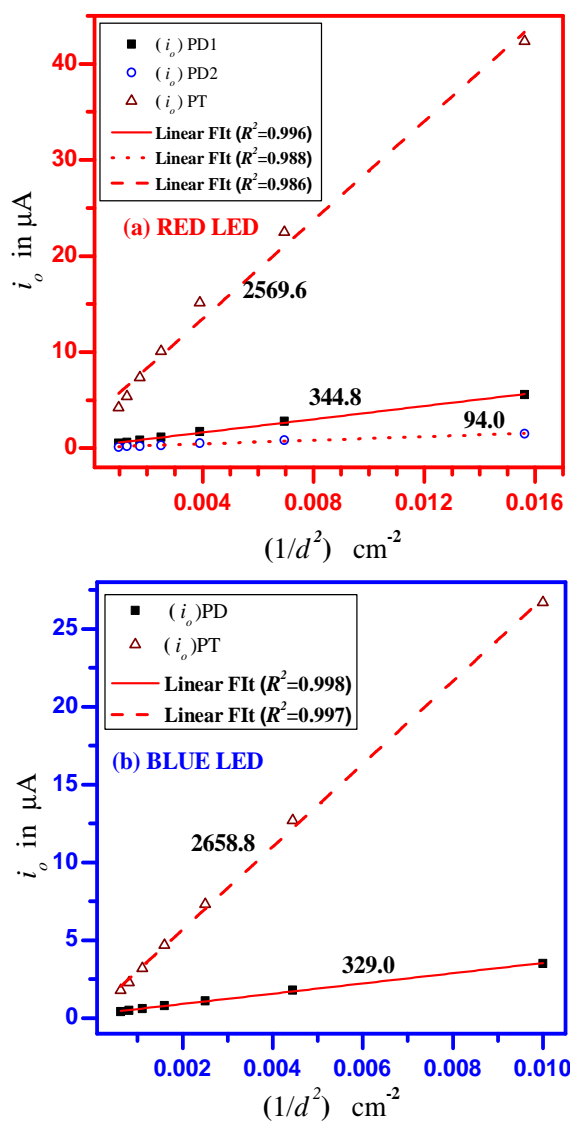
Figure 4: Plot of i_0 versus $1/d^2$ for (a) red LED measured with three detectors, viz., first photo diode (PD1-■), second photo diode (PD2- ○) and a photo transistor (PT-△) and for (b) blue LED with two detectors (PD1 and PT). Linear fit to data in both plots are done using Origin software.

unique for three detectors even with the same source. This indicates that the slope value is dependent on the type of detector used. Interestingly for a given detector, slope values 'k' with two different LEDs in figure 4(a) and 4(b) are nearly the same, which only shows that radiant intensities of red and blue LEDs are nearly the same.

Further, the method does not clarify which curve among the three, actually describes inverse square law of radiation. A close examination of plot reveals that, the linear fit to the data is imperfect. Therefore, the direct method does not reflect convincingly, correct behaviour of radiation in relation with distance. The second photodiode (PD2) has low output value as compared to the first one (PD1). Hence it is not used for further studies. A similar explanation holds good for the curves in figure 4(b). In some Indian institutions this direct method is used to verify the distance dependence of radiation and erroneously conclude that radiation describes inverse square law from an apparent straight line through the data.

Power Law Estimation:

For best illustration of the method, photo diode (PD1) data for blue LED's radiation is discussed here. The power exponent 'n' of distance with radiation is obtained from the plot of $\log i_0$ versus $\log d$ as ≈ 1.72 (figure 5(a)). This is lower than the expected value of 2.00. This shows that an apparent straight line fit to the data as in the direct method does not reflect inverse square law behaviour. One of the reasons for this discrepancy, is suspected to be in the measured d value. Since d is measured between the tip

of LED and the tip of detector according to the published literature [2, 8]. Exact location of light emission in LED and exact location of light detection in the detector are different to the measured d. Therefore the measured separation distances need corrections.

To make an estimation of correct separation distance, a plot of $[1/(i_0)^{1/2}]$ versus d is drawn (figure 5(b)). If the measured 'd' values are correct, then a straight line fit to data must pass through (0,0) point in this plot, which in most cases do not happen. The fit line is extrapolated to obtain intercept along d. This gives a measure of distance 'd_c' needs to be corrected, which is '-2.10' cm for the case studied. A negative d_c indicates an under estimation of measured separation distance. This sign is acceptable here, as the separation distances are measured between the tip of LED and the tip of detector. Then correct separation distance r between LED and the detector is calculated as, $r = d - d_c$. If $d_c < 0$ then $r > d$ and vice versa. An over estimation of distance d would give a positive d_c value. With correct distance r, (2) changes to a new relation,

$$E = I/(d - d_c)^2 = I/r^2 \qquad (6)$$

With this correction, $r > d$, data points shift towards higher d values in a plot of $\log i_0$ versus $\log r$ as compared to the previous case (figure 5(a)). It is found that the effect of d_c on d is more at shorter distances as they are of same order than at longer distances. This correction changes the slope of the curve to 2.01±0.042.

By using two detectors (PD and PT), this

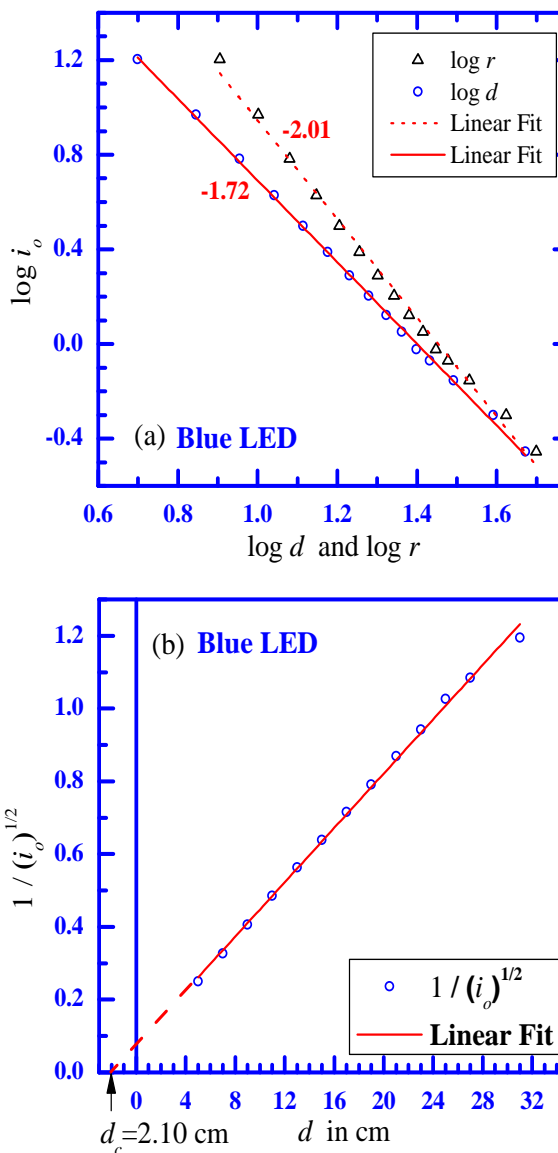
Figure 5: (a) Plot of $\log i_0$ versus $\log d$ (O) and $\log i_0$ versus $\log r$ (△) for blue LED as measured by a photo diode and (b) A plot of $1/(i_0)^{1/2}$ versus d to determine correction distance d_c.

analysis is repeated with all other sources mentioned in the section 3 and the results are

Source	Detector	n_{before}	d_c (cm)	n_{after}	R^2
Blue LED	PD	-1.72	-2.10	-2.01 ± 0.042	0.994
Red LED	PD	-1.68	-2.53	-1.99 ± 0.016	0.999
Blue LED	PT	-1.94	-0.60	-2.01 ± 0.014	0.999
Red LED	PT	-1.88	-0.98	-1.99 ± 0.023	0.999
LD (open)	PT	-1.88	-1.35	-2.01 ± 0.041	0.995
LD (open)	PD	-1.63	-3.84	-2.06 ± 0.053	0.992
IL	PD	-1.85	-4.66	-2.06 ± 0.017	0.997
IL	PT	-2.18	+3.08	-2.02 ± 0.026	0.999

Table 1: Fit parameters of curves in figure 6(a) as explained in figure 5.

shown in figure 6(a). For a given light source, PT data are shifted vertically upwards from PD data at all irradiances due to the gain G in PT.

The fit parameters of all the curves of figure 6(a) are given in table 1. In case of laser diode, distance is measured from the tip of the detector to tip of the casing in which laser diode is embedded. Therefore d_c values obtained are higher than those obtained with LEDs for both the detectors. In case of incandescent lamp (IL) with PD detector distances are measured between the tips of source and detector. With incandescent lamp and PT system, $n_{before} > 2.00$, due to the reason that distance is measured from the center of the bulb near filament to the tip of PT. This is carried out here to demonstrate that even a positive 'd_c' can result while correcting for separation distances. Since incandescent source is brightest among the sources, the measured distances are extended up to 140 cm from 15 cm. Importantly, these measurements with uncali-brated detectors demonstrates that even for isotropic radiators like IL, correction of d is necessary before using such systems for any other measurements that depends on inverse square law behaviour.

In table 1, the third and fifth columns give the exponent of distance 'n' before and after correction of the separation distance (d_c-fourth column) respectively. The n_{after} values for red LED being less than -2.00 even after correction in 'd' indicates a source of error. This source is suspected to be due to the presence of multiple peaks in red LED pattern leading to alignment error at all separation distances. The data of the sixth column gives the co-efficient of fit (R^2) to the n_{after} data set. A close proximity of R^2 to 1 indicates better the fit to data.

Nonlinear Curve Fit:

Instead of a linear curve, a nonlinear curve can be drawn for the same data and curve can be analyzed with the help of a computing system. The data set is normalized with the exposed area A of each detector and a modi-
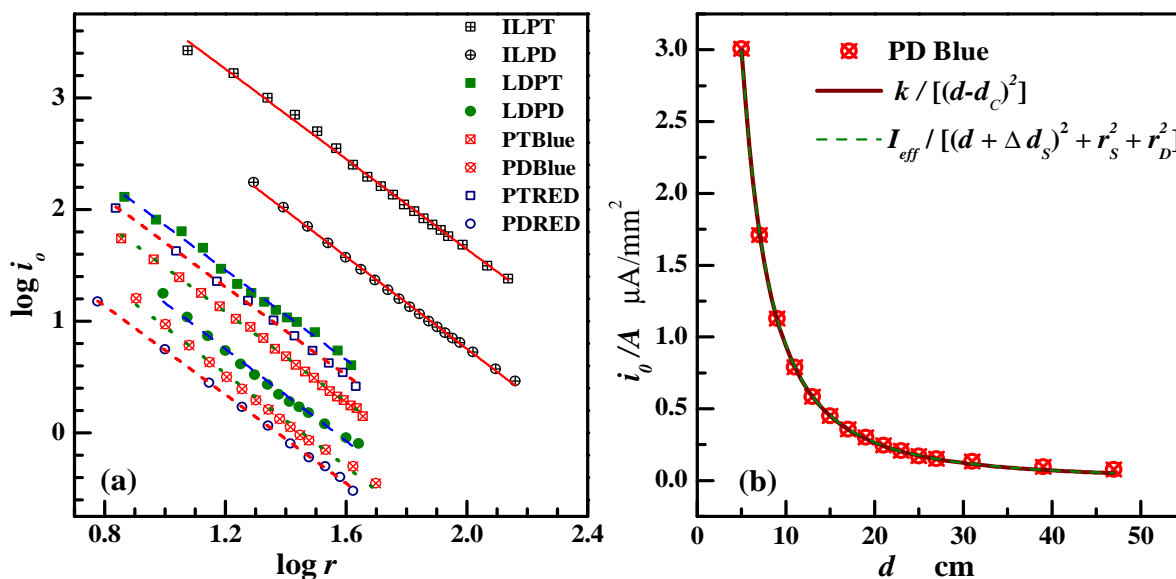
Figure 6: (a) Plot of $\log i_0$ versus $\log r$ with a photo diode (circles) and with a photo transistor (squares) for incandescent lamp ($\oplus$ and $\boxplus$), laser diode ($\bullet$ and $\blacksquare$), blue LED ($\otimes$ and $\boxtimes$) and red LED ($\circ$ and $\square$). (b) Plot of i_0/A versus d for a photo diode and blue LED system ($\otimes$). Data points are fitted with (7) (——) and with (8) (- - - -).

fied of relation (6) is used to fit the curve with free parameters 'd_c' and 'k'($\propto I$, intensity of radiation).

$$i_o/A = k/(d - d_c)^2 \qquad (7)$$

Figure 6(b) shows a nonlinear curve fit using (7) for the data obtained with PD and blue LED system. This procedure is extended for the remaining cases of measurement with LEDs and the results are given in table 2. Estimation of '$-d_c$' from power law method requires two plots whereas it can be obtained from a single plot with a nonlinear curve fit using (7). In addition, the latter method gives more reliable and reproducible values of '$-d_c$' due to the use of second free param-

eter k. Little more discussion on this topic is provided at the end of next section.

5.2 Applicability of the method

Detector output measurements are more accurate when they are closer to the source where it can receive a high percentage of radiation, whereas the measurements of 'd' are more accurate at large distances. In contrast, any actual source, barring collimated radiation sources like lasers, is of finite size. Due to finite size, irradiance from such sources describe the inverse square law of radiation provided the measurements with a detector are

LED	Detector	k (arb. units)	$-d_c$ (cm)
Blue	PD	$(1.197 \pm 0.017) \times 10^2$	1.32 ± 0.05
Red	PD	$(1.068 \pm 0.009) \times 10^2$	0.17 ± 0.03
Blue	PT	$(7.514 \pm 0.113) \times 10^3$	0.53 ± 0.04
Red	PT	$(1.390 \pm 0.021) \times 10^4$	3.24 ± 0.06

Table 2: Fit parameters 'd_c' and 'k' using (7) for all the curves in figure 6(a) as explained in figure 6(b).

carried out at a separation distance of about 10 times the size of the source [14]. This holds true whenever the dimensions of the source or of the detector are not small compared to d [5, 14].

It was shown that with calibrated detectors radiation from LEDs describe modified inverse square law [2, 5]. Therefore, in the process of determining the correction distance 'd_c' for a particular data set, it is assumed that radiation describes inverse square law. In power law method it is equivalent to forcing the distance data to describe inverse square law, but the method helps in estimating the error in d. However, reader is advised to be cautious because, in some systems this method can also yield spurious values of d. This can be identified with the knowledge of unaccounted length in d in such systems.

The sum of unaccounted distance in LED and in detector (PD or PT) from their tips is of the order of 1 cm. For such systems $d_c < 1$ cm. Measurements with PT satisfies this requirement here whereas those with PD do not for the same sources (see table 1). This encourages the use of a PT over a PD for any

further characterization of LEDs radiations. Therefore, a high value of d_c (> 1 cm) with PD implies the presence of a source of error inherent to PD other than d. Certainly, the measurements of separation distance 'd' reported here are carried out with a better accuracy using an optical rail having graduations of 1 mm. An attempt is made here to explain the discrepancy.

A method that takes into account of the effective sizes of source and detector while determining the nature of radiation using a modified inverse square law was developed by Manninen *et al.* This method is based on two aperture approximation of LED source and detector and the theory predicts that irradiance of LED source follow the relation [2, 10]:

$$E(d) = \frac{I_{eff}}{(d + \Delta d_s)^2 + r_s^2 + r_d^2} g(d) \quad (8)$$

Here, $g(d)$ is the multiplication factor which is close to unity; $d + \Delta d_s$ is the physical distance between the source and the detector; Δd_s is the offset distance of the source from its physical location due to encapsulation of LED; r_s and r_d are effective radii of

LED	Detector	I_{eff} (arb. units)	Δd_s (cm)	r_s (cm)	$(r_s)_{error}$
Blue	PD	$(1.193 \pm 0.053) \times 10^2$	1.30 ± 0.39	-4.26×10^{-5}	3.93×10^4
Red	PD	$(1.004 \pm 0.019) \times 10^2$	-0.41 ± 0.17	-2.13	0.29
Blue	PT	$(7.621 \pm 0.637) \times 10^3$	0.63 ± 1.85	2.51×10^{-4}	1.22×10^5
Red	PT	$(1.389 \pm 0.071) \times 10^4$	3.24 ± 0.55	-2.34×10^{-4}	1.14×10^5

Table 3: Fit parameters of the 'i_0/A' versus 'd' curves of all the LED's data in figure 6(a) (see figure 6(b) for blue LED and PD system) using (8) with $r_d = 0.035$ cm for PT and $r_d = 0.130$ cm for PD.

the virtual source and detector (aperture). For two LEDs and two detectors, plots of i_0/A versus d are drawn, and data are fitted using (8) with $r_d = 0.035$ cm for PT and $r_d = 0.130$ cm for PD with three free fitting parameters $I_{eff}, \Delta d_s$ and r_s. and results are shown in the table 3.

The condition required for an LED to serve as a point source is that, its encapsulation must behave as a moderate lens which is identified by the value of r_s parameter. If $r_s \approx 0$ then LED behaves as a point source [2].

Except red LED and PD system, all other systems produced $r_s \approx 0$, but with several orders of higher magnitude of uncertainty (sixth column of table 3). The uncertainty values of r_s for LEDs studied by Manninen *et al* were not reported [2]. The goodness of the fit to data with (7) in figure 6(b) requires that same data when fitted with (8), r_s value should approach zero in the latter method. It is believed here that, this requirement increases uncertainties in r_s values to very high level of the order of 10^5.

The results of table 3 indicate that blue LED behaves as a point source. In case of red LED and PD system $|r_s| > 0$ and $|r_s| > |\Delta d_s|$. They suggests that red LED does not serve as a point source [2]. However data with same red LED using PT provides $r_s \simeq 0$. This duality of results with red LED indicate a source of error that lies within PD [2]. This result of PD correlates with the earlier result obtained using power law method. Note that (8) is derived for a well calibrated detector. In case of an uncalibrated detector an improvement in the relation (8) is required with an additional term associated with the detector [15]. This term is defined as an offset of the detector's virtual plane position through certain Δd_D from the detectors aperture plane [15]. The effect of Δd_D on the measurements seems to be significant only on red LED and PD system. This Δd_D is not attempted to estimate here.

For a detector with a small pin hole aperture $r_d \ll d \approx 0$ and with $r_s \approx 0$, (8) reduces to (7) with $\Delta d_s = -d_c$. Figure 6(b) illustrates the fitted curves to data by (7) and by (8) for PD and blue LED system. These fitted curves found to overlap each other in the figure 6(b). This suggests that the assump-

tions, viz., $r_d \approx 0$ and $r_s \approx 0$ are valid.

The use of two fitting parameters in (7) and three in (8) with $r_s \approx 0$, seems to produce values of k to be in fair agreement with I_{eff}. Also, '$-d_c$' is in fair agreement with Δd_s, in all the systems studied. Importantly, the magnitude of uncertainties in all the fit parameters are smaller using (7) than that using (8). Therefore for LEDs with low value of r_s, and one can use the simplified relation (7) instead of (8) for obtaining better results.

Optical power radiated or external efficiency of an LED are inherent properties of that LED. In an undergraduate laboratory, they are determined by placing a detector at certain separation distance from the source. Therefore, these properties of LEDs depend mainly on the power law behaviour of LED's radiation. Whenever ordinary detectors are used for measurements then following precautions must be taken care of:

1. Alignment of peak irradiance along the direction of measurement.

2. Ensure that LED being probed has an angular distribution ($\theta_{1/2}$) value greater than $10°$.

3. Use either power law or nonlinear curve fitting methods to know the true working of systems along beam propagation direction.

4. When power law method is used, then make sure that a prior knowledge of unaccounted distance between source and detector is in hand.

When external efficiency of an LED measurements are carried out, an unambiguous efficiency of blue LED is obtained with a photo transistor at all separation distances above 7 cm, suggesting that inverse square law of radiation is described by that system only at seperation distances d above 7 cm [16].

The exponent of distance n_{after} in all the measurements (fifth column in table 1) is nearly -2.00 with margin of error shown. This suggests that even anisotropic radiators like LED and diverging laser exhibit inverse square law behaviour. The power law method holds good even for an isotropic radiator like incandescent lamp. Therefore it is extended for β and γ nuclear radiations using a GM detector (results are not shown) and method's validity for nuclear radiations are also tested.

6 Conclusions

The radiation emitted by anisotropic radiators like LEDs were studied using inexpensive photo diode and photo transistors in three dimensions. In the direct method, it was shown that slope k value depends mainly on the detector type used, however the method do not provide the true nature of relation between radiation with distance. In the power law method, it was found that with a prior knowledge of expected correction distance d_c for a measuring system, one can identify a detector that reproduces inverse square law of radiation to the best extent. In the present study photo transistor does satisfies this requirement. Further, it was shown that

knowledge of peak irradiance position from an anisotropic source is necessary to obtain better results. Limitations and validity of the power law verification method were discussed. Any uncalibrated detector can be tested on its working ability with this procedure. If nonlinear curve fitting for the data is feasible, then two aperture approximation method or its simple version in the form of relation (7) can be sued. Essentially, (7) was found to five better results with lower errors in the fit parameters for LED's with $r_s \approx 0$ and with $\theta_{1/2} > 10°$.

Acknowledgments

References

[1] Hecht E 2002 *Optics, 4ᵗʰ Edition* (Pearson Education Inc, New Delhi) p 50

[2] Manninen P, Hovila J, Kärhä P and Ikonen E 2007 *Meas. Sci. Technol.* **18** 223

[3] Moreno I and Sun C C 2008 *Opt. Exp.* **16(3)** 1808

[4] Moreno I 2006 *Proc. SPIE* **6342** 634216

[5] Wanser K H, Mahrley S and Tanner J 2012 *Phys. Edu (UK)* **47(2)** 174

[6] Rajesh B K and Smitha P 2007 *Phys. Edu (India)* **23(4)** 291

[7] Kutzner M, Wright R and Kutzner E 2010 *Phys. Teach.* **48** 341

[8] Kasap S O 2011 *Optoelectronics and Photonics-Principles and Practices, 1ˢᵗ Edition* (Pearson Education Inc, New Delhi) p 6, p 13, p 225

[9] Nelkon M 1977 *Fundamentals of Physics, 3ʳᵈ Edition* (Hart-Davis Education Ltd., Hertfordshire) p 448

[10] Kärhä P, Manninen P, Hovila J, Seppälä L and Ikonen E 2005 *Proc. NEWARD2005* p 211 available at `http://www.pmodwrc.ch/neward2005/pdfabstracts/newrad044.pdf`

[11] Specifications of mounted optoelectronic devices from the supplier Holmarc at `http://holmarc.com/mounted-optoelectronic-components.html` retrieved on 08-07-12 and private communication.

[12] Wieman C E and Hollberg L 1991 *Rev. Sci. Instrum.* **62(l)** 1

[13] Sze S M and Ng Knok K 2007 *Physics of semiconductor devices, 3ʳᵈ Edition* (Wiley India (P) Ltd. New Delhi) p 696

[14] Kruglak H 1975 *Am. J. Phys.* **43** 449

[15] Manninen P, Kärhä P and Ikonen E 2008 *Appl. Opt.* **47(26)** 4714

[16] Raghu A *Unpublished data- manuscript under preparation.*

The Inverse Square Law and Near Field Communication

A. Braeken[1], P. Leemans[1], and Mark Vanophalvens[2]

[1]Department of Industrial Engineering
Vrije Universiteit Brussel
Nijverheidskaai 170, Brussel, Belgium

[2]Atos WorldLine
Brussel, Belgium.

Abstract

Near field communication (NFC) is a short-range wireless communication technology, very popular in identification and payment systems. Resistance against different types of security attacks requires the existence of a secure channel. Instead of using operational intensive cryptographic computations, a secure channel can be theoretically obtained based on the superposition principle when sender and receiver send a signal at exactly the same time. In this paper, we show that due to the inverse square law, the attacker can clearly identify the signal of the most nearby device if (s)he is not exactly placed in the middle.

1 Introduction

NFC is based on Radio Field Identification (RFID) technology. It is designed for short and quick transactions, which are reduced to simply touching or bringing devices in close proximity. Due to the success of the smartphone, the NFC technology experiences a tremendous growth, with popular applications such as advertising tags, banking transactions, tickets,...

Despite the fact that NFC only supports short communication ranges, it does not mean that it is resistant against security attacks such as eavesdropping, data corruption, data modulation, denial of services and relay attacks [1],[2]. The existence of a secure channel to share a secret key is an essential re-

quirement for offering resistance against these attacks. It is used as basis for many security protocols to continue the rest of the communication. Instead of using expensive cryptographic operations, Haselsteiner and Breitfu [1], propose the idea of establishing a secure channel based on superposition, but never tested it practically.

In superposition, both devices A and B, send a different bit at exactly the same time by amplitude shift keying (ASK). An attacker cannot distinguish which bit is coming from whom due to superposition of both signals. When both devices send the same value, these bits are discarded. It should be decided upfront, whose bits are collected. Consequently, when a 256-bit signal is sent, an approximately 128-bit secret will be constructed. Fig 1 illustrates this effect.
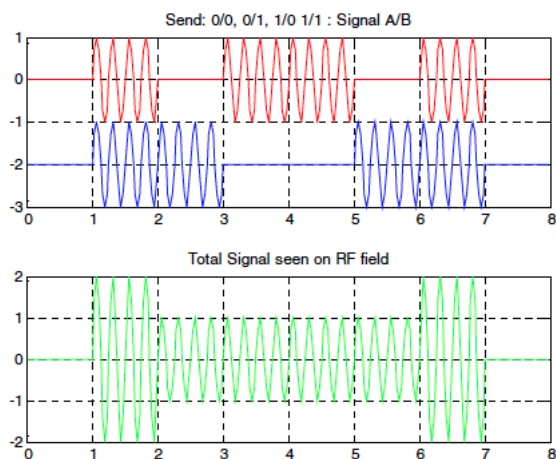

Figure 1: PResult of superposition of two signals, send by ASK [1]

To check the efficiency of the proposed secure channel, we work with the peer-2-peer

mode, being both active devices for sender and receiver when sending data. So, there will be no difference in signal strength.

2   Experimental setting

Two devices, A and B, send in active mode and receive when the RF field is deactivated. Consequently, both signals contain the same amplitude, and thus exclude any possible irregularity. Another device S, also called spy, will receive and collect the data of A and B, while A and B are sending simultaneously data. The spy is configured as passive device, does not generate any RF field, and only receives data. Therefore, the spy will have no influence on the RF fields or data send by the terminals A and B. After synchronization, we ensure that the devices constantly send data, so no measurement data losses can occur. Both terminals will continue to fill their FIFO buffer with their respective signals during submission.

3   Results

We consider 4 situations with 25, 20, 10 and 5 centimeters distance between A and B. In all 4 situations, we vary the position of S and analyze the result. From all the experiments, we conclude that if the position of S is closer to either A or B, the exclusive signal of A or B respectively is picked up. Also behind the devices, the result corresponds with the pure signal of that device.

Only in the middle over a range of 5 cen-

timeters, a mix of different signals occurs, where the superposition signal reaches the highest probability. These results are easily explained due to the inverse square law, describing the inversely proportional relation of the signal strength to the square of the distance from its source. Consequently, only in the middle, the same signal strength for the two signals occurs. Fig. 2 presents the intensity curve of the signal between A and B at a distance of 25 centimeters from the experiments. The signal strength at different distances was measured with an oscilloscope. If the distance between S and A equals to 5 centimeters, the signal strength corresponds to 760 mV. At B, the signal strength is already decreased to 43 V. Consequently, it is clear that S will not even notice the signal of B, since the signal strength of A is approximately 16 times larger. As we are dealing with ASK, the amplitude determines the value of the signal.
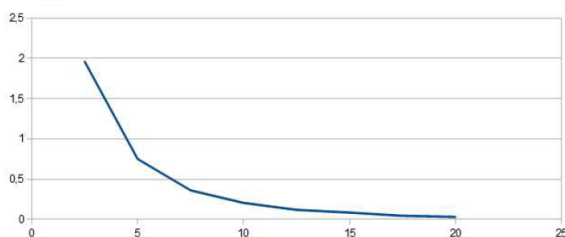

Figure 2: Intensity curve (V) related to distance (cm) for a signal between 2 devices at 25 centimeters distance.

4   Conclusions

Due to the signal strength inverse law, superposition between 2 devices is only obtained in the middle over a range of 5 centimeters. As a consequence, we can conclude that the NFC key agreement protocol, as theoretically proposed in [1], will not be secure. Very recently, Wang et. al. [3] show how randomizing the modulation and the channel can successfully establish a secure channel. Consequently, there seems to exist possibilities to realize a secure channel without cryptographic techniques. However, more research is required in effectively checking these techniques.

References

[1] E. Haselsteiner and K. Breitfu (2006), Security in near field communication (NFC), in Workshop on RFID Security RFIDSec, 2006.

[2] P. S. Halgaonkar, S. Jain, and V. M. Wadhai (2013) NFC: A review of technology, tags, applications and security, IJRCCT, vol. 2, no. 10, pp. 979987.

[3] J. Wang, H. Hassanieh, D. Katabi, T. Kohno (2013) "Securing Deployed RFIDs by Randomizing the Modulation and the Channel", Technical Report, Jan 2013.

Getting High School Students Excited about Physics

M.J. Ponnambalam

Physics Department
University of the West Indies
Kingston 7, Jamaica

michael.ponnambalam@uwimona.edu.jm

(*Submitted* 19-12-2014)

Abstract

The Laws of Physics are objective and may seem "cold" to some people. However, their presentation is subjective, and can vary from being "very boring" to "very exciting." When the presenter enjoys Physics, has a passion for it, and sings as well as dances Physics in the wavelength, vocabulary and emotional domain of the students, they experience an enjoyable excitement and discover for themselves that "Physics is fun." The author's presentations in several Western countries testify to this. The experience of the author in August 2014 with 310 High School students from Mumbai, as well as the lessons from that encounter is presented in this paper.

Introduction

Physics was born at the dawn of creation, when our ancestors looked at the moon and the stars, and marveled at the beauty, harmony & wonders everywhere. Physics is just a serene contemplation of Mother Nature – the beauty, truth and power in her. As Zukav [1] puts it: "Physics, in essence, is simple wonder at the way things are, and a divine interest in how that is so. … Physics become pure enchantment." In 1934, Einstein spoke of his "rapturous amazement at the harmony of Natural Law" in his book, "The Religious Spirit of Science."How do we communicate to the world the real Physics i.e. Zukav's 'pure enchantment' and Einstein's 'rapturous amazement'?

The Problem

In every country in the world, it is not unusual to hear comments like: "Physics is hard. Physics is boring. I don't like Physics." If Physics is 'enchanting' to Zukav (who is not a physicist), how does it become 'boring' to the students in Colleges and Universities? More than 35 years of experience of the author in Teaching, Research and Outreach in 4 continents has revealed that the poor communication skills of the Physics teachers, as well as the fun-focused materialism of the modern world, play a major role in the formation and growth of the prejudice as well as the brainwash, that Physics is hard and boring.

The Solution

On the positive side, the author has observed the following in his Physics Outreach in Belize (Central America), Grenada (West Indies), India, Jamaica (West Indies) and Trinidad (West Indies): "The younger students in High Schools don't have such prejudice. They enjoy Science/Physics and are very open to it." Hence, while getting the brain-washed grown-ups excited about Science/Physics is a difficult job, requiring a lot of time & money, doing the same for the High School students is an easy job. Further, the curiosity and inquisitiveness of the younger ones are worth comparing with the words of Einstein [2]: "I don't have a special talent; only a passionate curiosity." This reveals the enormous potential of any country, hidden in its High School students. Indeed, any country's future Einsteins are right there in its High Schools – waiting for their 'child-like curiosity' to be fanned into an 'Einstein's passionate curiosity'.

The "Interactive Show on 'Physics/Science Is Fun' " is an attempt in this direction. It follows faithfully the words of wisdom of the Director of Public Affairs of the American Physical Society, Michael Lubell [3]: "Establishing an emotional connection is an essential precursor to communicating serious information. Lighting up the amygdala gets the rest of the human brain to pay attention." Thus, in the Interactive Show, attention-grabbing, toy-like demonstrations are used in a highly active and interactive way to create a sense of 'wonder'. This is followed by a simple, Physics-based explanation. The students go through 'an intense immersion experience in Physics'. They come out with an enjoyable excitement and the discovery that Physics is fun.

Special Practices

The philosophy of the Show is summarized in the mantra: *"Taste and see that 'Physics is fun'."* The focus is on 'tasting' – and not on 'reading', 'hearing', or 'seeing'; not even on 'learning'. Everything is adjusted so as to enable the students to 'taste' Physics and to experience Zukav's 'pure enchantment' and Einstein's 'rapturous amazement'. The following steps are helpful in achieving the above:

i) The class size is kept small, around 30 students at a time, to facilitate close interaction.
ii) Every student is given a chance to come to the front of the class for some activity.
iii) During the activities, the students are given the freedom to touch, feel, play, talk, explore, discover, experience, enjoy, exclaim, …
iv) The presenter is a passionate lover of Physics.
v) He/she moves around, getting close to every student at some time or other.
vi) He/she bubbles with an infectious enthusiasm and boils with explosive energy.
vii) He/she sings, dances and tells stories in the wavelength and vocabulary of students.
viii) He/she dramatizes things, whenever possible

High School Children in Mumbai

In August 2014, the author was invited to conduct the Interactive Show to 7 Divisions/Sections of 6th Standard students in Gokuldham High School, Mumbai. Each Division had 45 – 50 students. Since it was difficult to split the Divisions into Sub-Divisions, the Show was conducted for two class-periods (60 minutes) to one Division at a time. 305 students completed the Evaluation Form. The results are summarized in Figures 1 to 3, where percentages less than 10 are given correct to a decimal.
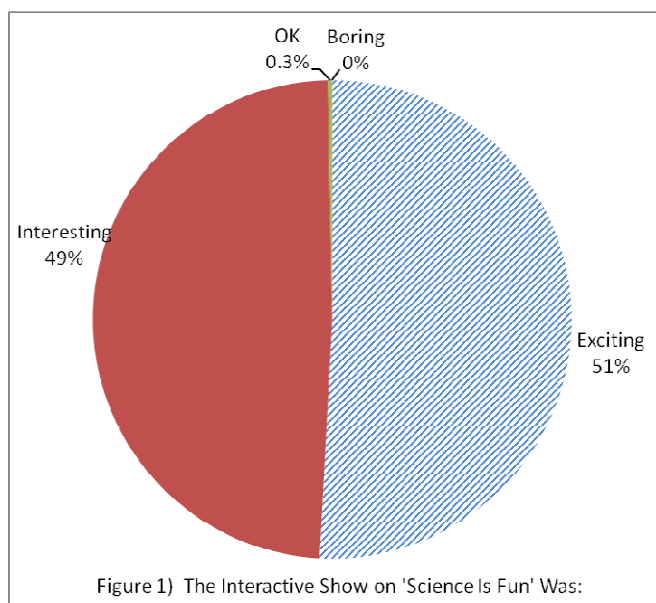
Figure 1) The Interactive Show on 'Science Is Fun' Was:

Figure 1 shows that 51% of the students found the Show 'Exciting', and another 49% 'Interesting'. Only one student (0.3%) had ticked 'OK', while no one found the Show 'Boring'. This confirms the earlier statement that the younger ones are not contaminated by the prejudice that Physics is hard and/or boring.
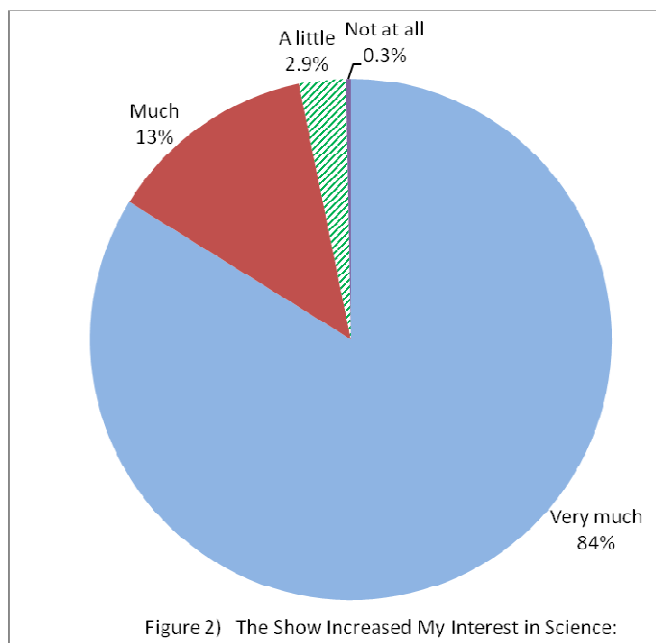

Figure 2) The Show Increased My Interest in Science:

Figure 2 is a check on whether the Show increased the students' interest in Science/Physics. 84%

have ticked 'Very much' and 13% 'Much' – totaling an impressive 97%. This is a verification of the following words of Alan Chodos[4], Associate Executive Officer of the American Physical Society: "If we could get members to go to K-12 schools and levitate a magnet or something, we really think these efforts would bring great rewards." Further, 97% of the students have mentioned that they would recommend this Show to their friends. All these reveal the enormous power and potential of the Interactive Show to fan the 'child-like curiosity' of the students into an 'Einstein's passionate curiosity'. These show that, with proper guidance, the Indian students are capable of winning the Nobel Prize in Physics, when they grow up.

In the earlier questions, the students tick one of the answers given. In the final question, they are requested to describe the Show in their own words. The response is summarized in Figure 3. The top 4 responses are: 'Very Interesting' (30%), 'Educational' (18%), 'Exciting' (17%) and 'Fun' (14%) – totaling 79%.
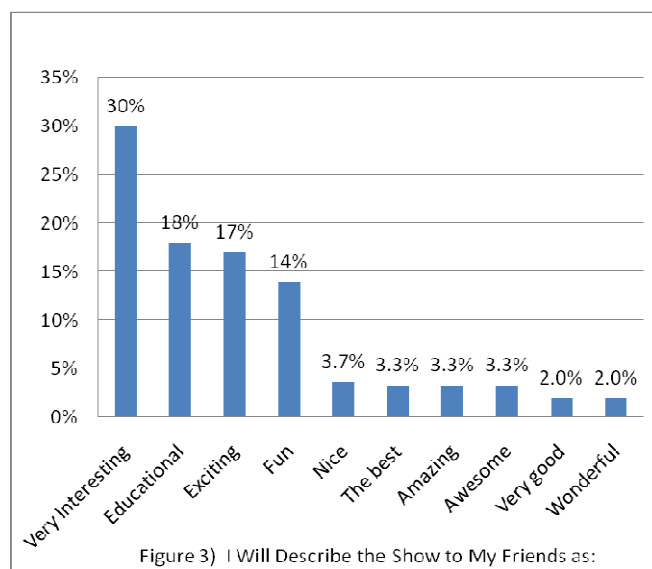

Figure 3) I Will Describe the Show to My Friends as:

This proves that Science education can be very interesting, exciting and fun-filled – at least at the early High School level. The next 6 responses are: Nice, The best, Amazing, Awesome, Very good

and Wonderful. Other descriptive words are: Cool, Fantastic, Fabulous, Great, Memorable, Mind-blowing, Outstanding and Superb. The interesting statements below are also found among the responses:

- The Show was very interesting & it increased my interest in Science. (111 students)
- I liked/loved the Show very much. (69 students)
- It was a very exciting Show. (39 students)
- I enjoyed the Show very much. (29 students)
- I thought that Science was boring. Now I know that it is interesting. (24 students)
- I never thought that Science was so interesting. (19 students)
- It was the best Show I have ever seen. (16 students)

India on Top of the World

During the Show, the presenter/author tells the students that it is time for India to become 'Number One in the World', and invites them to work together for turning the 21st century into the 'Indian Century'. The following statements from 3 students affirm that India will become Number One soon: i) The Show was very interesting. In fact, I don't have enough words to describe it. I always disliked Science; but from now on, I love Science, and I want India to be no. 1 in the world." ii) It was an amazing experience. The uncle was very nice. I loved the experiments. They were very interesting. I am sure we will see our India at no. 1 position very soon. iii) I would like to become a scientist and help India to be 'Number One in the World'.

Conclusion

The Laws of Physics are very objective, and hence may appear cold to many people. However, the presentation of these can be very warm, lively, passionate – and even dramatic and poetic – if the presenter has a passionate love for Physics, an infectious enthusiasm and expert communication skills. The poet Lord Byron [5] is right when he said: "There's music in all things" – including Physics. Kenneth Laws [6] says that 'dance' is full of Physics. More interesting is the fact that Physics is full of dance – the dance of the electrons around the protons, the dance of the atoms in the vibrations of solids, the dance of the Earth around the Sun, etc. It is a great privilege to communicate the music, the dance, the drama, the wonder, and the excitement in Physics to the students. The younger ones in the High Schools have not been infected by the prejudice that Physics is hard and boring. They are very curious and open-minded. Physics Outreach to this age group takes much less time and money than to those in Colleges and Universities – and yet yields much better results. Enabling the younger ones in India today to "taste and see that Physics is fun" may well be the royal road to getting more Nobel Prizes in Physics in the future.

References

[1] G. Zukav, *The Dancing Wu Li Masters*, Bantam Books, New York, p.4 (1979).
[2] M. Fluckiger, "Albert Einstein and Switzerland," Albert Einstein Society, Berne, p.3 (1991).
[3] M. Lubell, American Physical Society/APS News, Vol. 16, p. 6 (December 2007).
[4] A. Chodos, American Physical Society/APS News, Vol. 14, p. 8 (January 2005).
[5] Lord Byron, Don Juan, Canto XV, Stanza 5.
[6] K. Laws, Physics Today, Vol. 38. No. 2, p. 24 (1985).

Physics Through Laboratory:
Determination of Magnetic Dipole Moment of Permanent Disc Magnet with Two Different Methods

D. Amrani

Physics Laboratory, Service des Enseignements Généraux,

École de Technologie Supérieure, University of Quebec,

1111, Rue Notre-Dame Ouest, Montreal (QC) H3C 1K3, Canada

E-mail: djilali.amrani@etsmtl.ca

Abstract

In this work, we present two different experiments to estimate the magnetic dipole moment of cylindrical neodymium magnets, which can be used by physics teachers and students at college or university level. One experiment is using computer data acquisition system and sensors to record measurements in real time. And the other one is employing a precision digital balance and meter-stick to measure the force between two the magnets. The magnetic dipole moment is determined from the slope of the magnetic force as a function of the inverse fourth power of the distance. The estimated average magnetic dipole moment by force sensor and digital balance is 1.5 ± 0.05 Am^2 and 1.29 ± 0.04 Am^2, respectively. The experiments details are described and the results discussed.

1. Introduction

The magnetic force interaction between two magnets is beyond monopole-monopole interaction; it is considered magnetic dipole-dipole interaction. This relevant topic is discussed in many text books of electricity and magnetism [1].

In this paper, we present two different experiments to investigate the relationship between the magnetic force as a function of the distance of separation between two identical disc neodymium magnets, and to estimate the magnetic dipole moment of permanent magnet.

The first proposed experiment uses a computer data acquisition system and commercially available sensors of Pasco [2],wherethe data of themagnetic force as a function of distance

of distance between the two magnets are recorded and plotted graphically in real time measurements.

The second one is classical experiment that employs a precision balance with a digital readout measurement of the force between two magnets as a function of distance.

The magnetic dipole moment of permanent magnet, for both methods, was determined from the slope of the linear best fit of the graph representing magnetic force versus inverse fourth power of the distance of separation between the two magnets. The experimental details of both experiments are described and the results are discussed.

The simplicity and relatively small laps of time to perform data measurements of the activities presented in this work can probably contribute to creating appropriate learning environments and promote the successful students learning of magnetic concepts.

2. Force between two disc magnets

The magnetic force between two identical disc magnets with the vectors of magnetization lying on their common axis was approximated by the expression[3].

$$F(x) = \frac{\pi \mu_o M^2 R^4}{4} \left[\frac{1}{x^2} + \frac{1}{(x+2h)^2} - \frac{2}{(x+h)^2} \right] (1)$$

Where $\mu_o = 4\pi \times 10^{-7} \ TmA^{-1}$ is the magnetic permeability, M the magnetization of the magnets, x the distance of separation between the two magnets, h the thickness (height) of the magnets and R the radius of the magnet.

The effective magnetic dipole moment is expressed as,

$$m = MV \qquad (2)$$

Where, V represents the volume of the magnet. For a cylindrical magnet $V = 2\pi R^2 h$. In the case

where $x \gg h$, the expression (1) reduces to the following.

$$F(x) = \frac{3\mu_o m_1 m_2}{2\pi} \cdot \frac{1}{x^4} \qquad (3)$$

This relation demonstrates that the magnetic force is proportional to the inverse fourth power of the distance between the two magnets. The magnetic dipole moment, m, can be determined from the slope of the plot of magnetic force versus the inverse fourth power of the distance.

3. Experiments and procedures

3.1. Computer-aided experiment

This experiment is based on the use of computer data acquisition system and commercially available force and rotary motion sensors. The force sensor is to measure the magnetic force of the magnet and the motion sensor indicates the distance of separation between the disc magnets.

Data measurements obtained by both sensors were recorded and displayed graphically in real time. The magnetic dipole moment of a permanent neodymium magnet was determined after the magnetic force as a function of distance between two identical disc neodymium magnets was performed by means of the experimental setup, as shown in Fig.1.
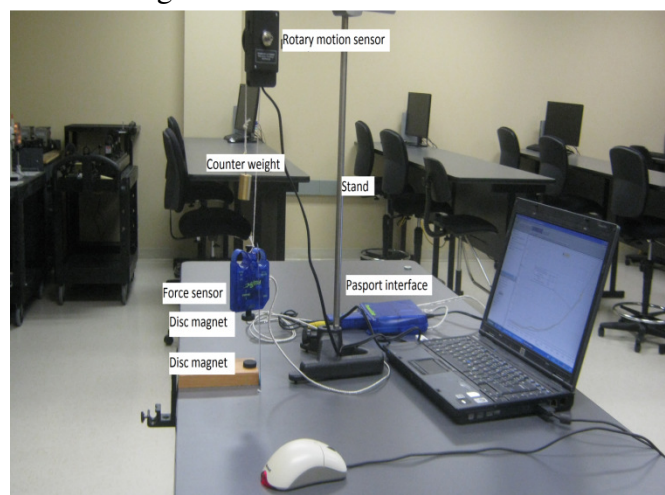
Fig.1. Experimental setup, showing computer data acquisition system, force and motion sensors, and dic magnets.

In this work, we used modified experimental procedure analysis and apparatus that are employed by [4].Two identical disc neodymium magnets, magnetized through the thickness, of volume (12.7 x 12.7 x 6.35 mm^3) were used to investigate the magnetic force as a function of distance between them and to estimate the magnetic dipole moment of the magnet. One of the magnets is glued on a table and the other magnet is fixed to the *Pasport force sensor* of Pasco. The two discs are placed in repelling position. In order to measure the exact distance of separation between the two magnets, a *rotary motionsensor* of Pascois placed on a stand, this unit has three pulleys on it of different diameters, 10 mm, 29 mm and 48 mm (*three-step pulley*). A cord is wrapped around a medium pulley of this sensor, one end of the string is connected to a counterweight mass of 200 g and the other end is attached to the *force sensor*. The two sensors were connected to the computer via the *Pasport interface* of Pasco; where data measurements are recorded, displayed and analyzed in real time using *Datastudio software* of Pasco.
A file is created in *Datastudio*to display graphically the vertical magnetic force as a function of distance of separation between magnets. The sampling rate of *force* and *rotary motion sensors* are set at 10 Hz, the sensitivity of both of them is adjusted at *Low,* and for a linear calibration of medium pulley of the rotary motion sensor a *360 divisions/rotation* was chosen for this purpose.
The force sensor with the magnet is pushed smoothly from a height of approximately 12 cm down to about 3 cm away from the fixed magnet on the table. At this distance, i.e., 3 cm the pushing repulsive force is more powerful. A graph representing a plot of data measurements of magnetic force as a function of distance of separation is shown in Fig.2. As can be seen from this graph, the magnetic force varies inversely as

the fourth power of the distance with a power exponent $n = - 4.02$.
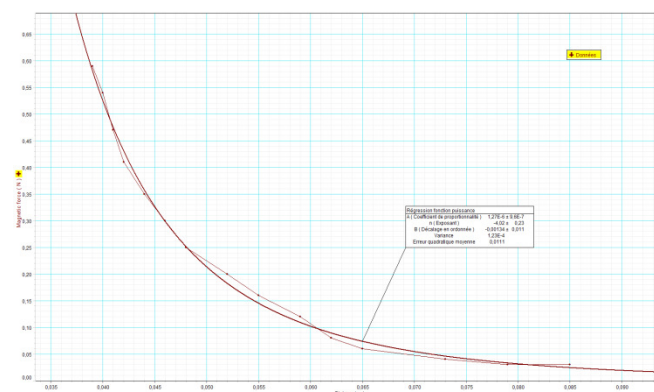
Fig.2. Magnetic force vs. distance − Computer-aided measurements.

3.2. Balance and meter-stick experiment
A digital balance of 0.01 g of precision and meter-stick are used in this experiment to explore the magnetic force as a function of distance between two identical disc neodymium magnets, as shown in Fig.3,the same magnets are employed as in the computer-aided experiment. One of the magnets is taped onto the balance pan, and the other magnet is fixed to the end of the meter stick, near the zero mark, with transparent glue. These magnets are placed in repulsive position, and the meter-stick was held by a clamp mounted onto a stand. A reference point is created in the meter and data measurements are performed in the interval of 3 to 18 cm of separation between discs with a 1 cm increment.

The graph of data measurements of magnetic force versus distance of separation between the two discs magnets is shown of Fig.4. The best fit data of this plot is a curve of inverse fourth power, with a power exponent $n = - 3.882$ and coefficient of determination $R^2 = 0.9994$.
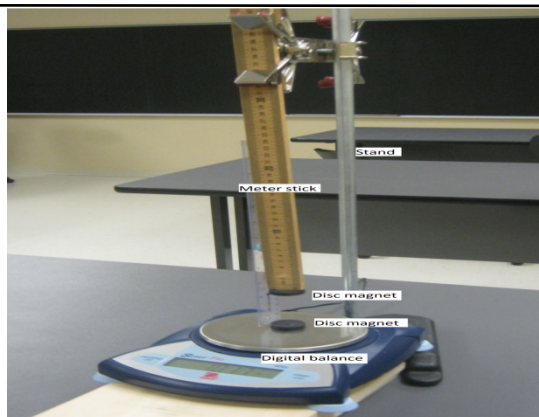
Fig.3. Experimental setup – Digital balance and meter stick

4. Results analysis and discussion

In order to correct systematic errors, special attention is paid when calculating magnetic forces F whichare obtained from the measurement of the masses displayed on the digital balance and so in the distance X between the two disc magnets as well. The estimated systematic error in the magnetic force ΔF and the distance of separation ΔX are 1.96 x 10^{-4} N and 2 x10^{-3} m, respectively. These systematic errors are taken in to account such that ΔF and ΔX are subtracted from F and X, respectively; when using equation (3).

In the absence of systematic errors, the mean value approaches the true (accepted) values as the number of measurements (trials) increases. To get the average value and the standard deviation of the magnetic dipole moment of the neodymium magnet, five trials are performed for each experiment, thecomputer-aided one and the digital balance-meter stick.
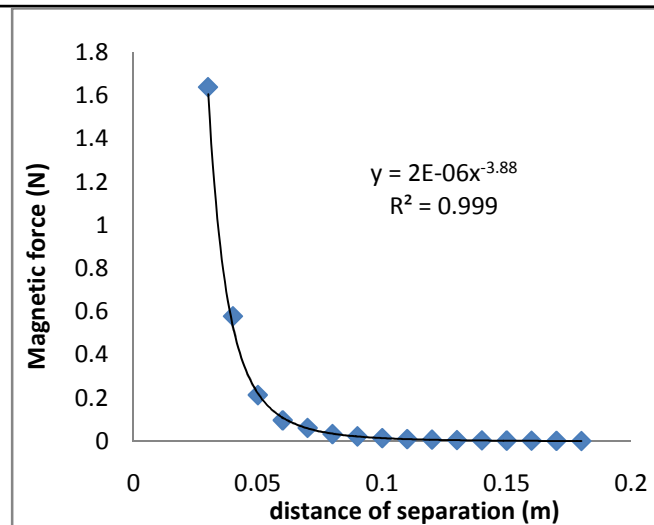

Fig.4. Magnetic force as a function of distance – Digital balance and meter-stick measurements.

As the magnetic dipole of the magnet is determined from the slope of the plot of magnetic force as a function of inverse fourth power of the distance between the disc magnets, the magnetic force versus distance between the two magnets are obtained for five trials for both experiments. Examples of graphs from the five trials of data measurements of magnetic force as a function of distance between the disc magnets for the computer data acquisition system experiment and the digital balance-meterstick are shown in Figure 2 and 4, respectively. As can be seen from these plots, the force varies inversely as the fourth power of the distance between the two magnets. The average value of the power exponent n, in equation (3), for the computer-aided experiment and the balance-meter stick one is - 4.05±0.16 and – 3.90±0.12, respectively. These results are in good agreement with the expected value closeto– *4*.

The data measurements of a force as a function of the distance are plotted as *log F* versus *log x* for the computer data acquisition system and balance-meter stick as shown in Fig.5 and 6, respectively. A linear best fit data is obtained for both experiments, the value of the slope, *m*, represents the power exponent, *n*, in equation (3).

Fig.5. Log force vs. log distance – Computer-aided measurements

Fig.6. Log force versus log distance - Balance –meter stick measurements

The magnetic dipole moment of disc neodymium magnet for each experiment is determine from the slope of the plot of the force as function of the inverse fourth power of distance.

Fig.7. Force vs. inverse fourth power of distance $(1/x^4)$–computer –aided measurements.

The slope $k = \dfrac{3\mu_o m^2}{2\pi}$, where m^2 is the magnetic dipole of the two identical disc neodymium magnets and μ_o the magnetic permeability. As can be seen from the plot of *force* versus $1/x^4$ the value of the slope for the computer aided experiment and the balance–meter stick one is 1.35×10^{-6} and 1.0×10^{-6}, respectively, as illustrated in Fig.7 and 8.

Fig.8. Magnetic force vs. inverse fourth power of distance – Balance –meter stick measurements

The average value of the magnetic dipole moment for five trials for the data acquisition system and the balance-meter stick experiments, is $1.50 \pm 0.05 Am^2$ and 1.29 ± 0.04 Am^2, respectively. The difference between these values is approximately 21%.

5. Conclusion

The experimental procedures and the results obtained by both experiments in this work provide a supplementary source of knowledge to college or university level students and teachers when exploring the relationship of the magnetic force in permanent cylindrical magnets. The other references are reported in literature [5].

The comparison between the two experimental methodsto estimate the magnetic dipole moment of disc magnet has confirmed that both of them are consistent due to their reproducibility in the same conditions. Both experiments can be performed in relatively small laps of time, and can be carried out as laboratory experiments by physics students or as demonstrationsin classrooms or laboratory by teachers. They investigate the relationship of the magnetic force-distance, the magnetic field-distanceand provide an estimate of the magnetic moment dipole of magnets.

The obtained results are found to be reliable andconsistent because the mean value of the magnetic moment dipole for five trials for computer aided experiment and balance meter-stick was 1.5 Am^2 and 1.29 Am^2 with standard deviation, σ $\pm 0.05 Am^2$ and ± 0.04 Am^2, respectively.

References

[1] D. J. Griffiths,*Introduction to electrodynamics,* 3rdedn (Upper Saddle River, NJ: Prentice-Hall), (1999)

[2] Pasco Scientific, 10101 Foothills Blvd, Roseville, CA 95747 7100, USA, http: www.pasco.com

[3] **321** 3758-3763 D. Vokoum, M. Beleggia, L. Heller and P. Sittner, *Magnetostatic interactions and forces between cylindrical permanent magnets,* J. Magn.Magn.Mater. (2009)

[4] Y. Kraftmakher,*Magnetic field of a dipole and the dipole-dipole interaction* Eur. J. Phys. (2007) **28** 409-414

[5] H. Sarafian, *Dynamic dipole-dipole magnetic interaction and damped nonlinear oscillations*J. Electromagnetic Analysis & Applications (2009)**1** 195-204